Research Paper

Hippocampal transcriptome profiling reveals common disease pathways in chronic hypoperfusion and aging

Sang-Ha Baik[1,2,*], Sharmelee Selvaraji[3,4,*], David Y. Fann[1,2], Luting Poh[1,3], Dong-Gyu Jo[5], Deron R. Herr[3,6], Shenpeng R. Zhang[7], Hyun Ah Kim[7], Michael De Silva[7], Mitchell K.P. Lai[3], Christopher Li-Hsian Chen[3,8], Grant R. Drummond[7], Kah-Leong Lim[9], Christopher G. Sobey[7], Thiruma V. Arumugam[1,5,7]

[1]Department of Physiology, Yong Loo Lin School of Medicine, National University of Singapore, Singapore
[2]Department of Biochemistry, Yong Loo Lin School of Medicine, National University of Singapore, Singapore
[3]Memory Aging and Cognition Centre, Department of Pharmacology, Yong Loo Lin School of Medicine, National University of Singapore, Singapore
[4]Integrative Sciences and Engineering Programme, NUS Graduate School, National University of Singapore
[5]School of Pharmacy, Sungkyunkwan University, Suwon, Republic of Korea
[6]Department of Biology, San Diego State University, San Diego, CA 92182, USA
[7]Department of Physiology, Anatomy and Microbiology, La Trobe University, Bundoora, VIC, Australia
[8]Department of Psychological Medicine, Yong Loo Lin School of Medicine, National University of Singapore, Singapore
[9]Lee Kong Chian School of Medicine, Nanyang Technological University, Singapore
*Equal contribution

Correspondence to: Thiruma V. Arumugam, Christopher G. Sobey; **email:** g.arumugam@latrobe.edu.au, C.Sobey@latrobe.edu.au
Keywords: aging, vascular dementia, transcriptome, chronic cerebral hypoperfusion, brain
Received: December 8, 2020 **Accepted:** May 11, 2021 **Published:** June 1, 2021

ABSTRACT

Vascular dementia (VaD) is a progressive cognitive impairment of vascular etiology. VaD is characterized by cerebral hypoperfusion, increased blood-brain barrier permeability and white matter lesions. An increased burden of VaD is expected in rapidly aging populations. The hippocampus is particularly susceptible to hypoperfusion, and the resulting memory impairment may play a crucial role in VaD. Here we have investigated the hippocampal gene expression profile of young and old mice subjected to cerebral hypoperfusion by bilateral common carotid artery stenosis (BCAS). Our data in sham-operated young and aged mice reveal an age-associated decline in cerebral blood flow and differential gene expression. In fact, BCAS and aging caused broadly similar effects. However, BCAS-induced changes in hippocampal gene expression differed between young and aged mice. Specifically, transcriptomic analysis indicated that in comparison to young sham mice, many pathways altered by BCAS in young mice resembled those already present in sham aged mice. Over 30 days, BCAS in aged mice had minimal effect on either cerebral blood flow or hippocampal gene expression. Immunoblot analyses confirmed these findings. Finally, relative to young sham mice the cell type-specific profile of genes in both young BCAS and old sham animals further revealed common cell-specific genes. Our data provide a genetic-based molecular framework for hypoperfusion-induced hippocampal damage and reveal common cellular signaling pathways likely to be important in the pathophysiology of VaD.

INTRODUCTION

Vascular dementia (VaD), like Alzheimer's disease, is a common cause of dementia [1] where there is an increased risk with aging, a rapid, step-wise decline in disease progression and a high mortality rate [2, 3]. While the root cause remains unknown, risk factors for VaD include diabetes, hypertension and metabolic syndrome [1]. As the current treatment options for VaD only address the symptoms, there is an urgency to better understand and treat the causes of this condition. Both clinical and experimental data indicate that cerebrovascular disease, as well as cardiac and systemic vascular diseases, may lead to cerebral hypoperfusion, thus altering brain metabolism and leading to cognitive impairment [4–8]. Indeed, cerebral hypoperfusion-induced microscopic infarcts (microinfarcts) and white matter injuries are common in VaD patients [8]. However, the mechanisms by which cerebral hypoperfusion-induced microinfarcts promote VaD remain unclear [9–12].

In order to develop a mechanistic understanding of VaD development, this study has employed a mouse model of VaD consisting of chronic cerebral hypoperfusion caused by a surgically-induced bilateral common carotid artery stenosis (BCAS), a widely used model that induces subcortical ischemia [1, 13]. BCAS employs external microcoils around both common carotid arteries to reduce cerebral blood flow (CBF) and induce damage to the deep white matter. BCAS closely mimics several features of VaD in patients, including decreased metabolism, elevated inflammation, decreased blood brain barrier (BBB) integrity, white matter lesions, neuronal damage and working memory deficits [13, 14–17]. In particular, CBF to the hippocampus, a limbic structure pivotal in learning and memory and vulnerable to chronic stress [18], is reduced following BCAS [19], which is consistent with hippocampal atrophy in patients with subcortical VaD [14]. However, the transcriptional processes underlying this hippocampal susceptibility in VaD remain unknown. The present study has thus investigated the hippocampal gene expression profile of young and old mice subjected to sham surgery or BCAS for up to 30 days.

RESULTS

BCAS reduces cerebral blood flow and alters gene expression in the brain of young and old mice

Young (3 months old) and old (22 months old) male C57BL/6 mice were randomly assigned to receive either Sham or BCAS surgery (Figure 1A). CBF was measured at baseline level in Sham mice, immediately after BCAS surgery (BCAS 0D) and before euthanizing the animals at 7 or 30 days (BCAS 7D and BCAS 30D, respectively) (Figure 1B, 1C). CBF in all groups was expressed as a percentage, relative to mean CBF in young sham-operated mice at baseline (YSham). An age-associated decline in CBF was observed in old versus young sham-operated mice (Figure 1B, 1C). BCAS reduced CBF by ~30% initially in both young and old mice. It is notable that blood flow was similar in old Sham mice and in young BCAS mice immediately after BCAS surgery (BCAS 0D). Partial recovery of CBF was observed in young mice at days 7 and 30, whereas in old mice subjected to BCAS, CBF returned to the level recorded in old sham mice, albeit ~50% less than in young sham mice. These findings indicate that age-associated changes in CBF are profound and may be less impacted by additional partial carotid artery stenoses.

Unsupervised hierarchical clustering of differentially expressed genes (DEGs) in the hippocampus revealed significant differences between young and old sham-operated mice (Figure 1D). Heatmap patterns also varied in a time-dependent manner over 30 days post-BCAS surgery, as indicated by clustering. It is notable that the DEG heatmap patterns of OSham are similar to that of O7D and O30D BCAS mice.

Aging

There were 1688 significant DEGs (898 upregulated and 790 downregulated) between young and old sham-operated mice (Figure 2A). We annotated these age-associated DEGs by performing differential enrichment analysis using cluster profiling. Transcriptome analysis using gene ontology (GO) enrichment showed that the top 20 significantly upregulated GO terms in the old compared to young mice belonged to a myriad of development and cell migration processes, including angiogenesis, morphogenesis, cell adhesion, tissue migration and response to external stimulus (Figure 2B and Supplementary Table 1). Upregulation of GO terms such as tissue migration and antigen processing and presentation of peptide antigen also suggest upregulated immunological processes. The top 20 downregulated enriched GO terms for the old versus young mice belonged to physiological functions such as cell redox homeostasis, mitochondrial transmembrane transport, and key metabolic processes such as sulfur compound metabolic process, nucleoside triphosphate metabolic processes, ATP metabolic process, purine ribonucleoside metabolic processes, cellular respiration and protein folding (Figure 2B).

The top 50 upregulated genes in the old compared to young mice include mitochondrially encoded ATP

synthase membrane subunit 6 (*Atp6*), mitochondrially encoded cytochrome C oxidase III (*mt-Co3*), mitochondrially encoded cytochrome C oxidase II (*mt-Co2*), mitochondrially encoded NADH 4L dehydrogenase (*mt-nd4l*), genes involved in inflammation such as cysteine-rich angiogenic inducer 61 (*Cyr61*), early growth response 1 (*Egr1*), kallikrein related peptidase 6 (*Klk6*), salt inducible kinase 1 (*Sik1*), complement C4B (*C4b*), Kruppel Like Factor 4 (*Klf4*), apoptosis-related genes such as proto-oncogene, AP-1 transcription factor subunit (*Fos*) [20] and genes that regulate adult neurogenesis such as PH domain and leucine zipper 2 (*APPL2*) [21] (Figure 2C and Supplementary Table 2). The top 50 downregulated genes include, aldehyde dehydrogenase 1 family member A1 (*Aldh1a1)*, activin-binding follistatin (*Fst*) [22], anti-oxidative glutathione peroxidase 8 (*GPx8*) [23] and prostaglandin reductase 1 (*Ptgr1*) [24], sulfotransferase family 1A member 1 (*Sult1a1*) and ATPase secretory pathway Ca^{2+} transporting 2 (*Atp2c2*) that modulate phonological short-term memory in language impairment [25] and a gene encoding a member of a family of adenosine triphosphate (ATP)-metabolizing molecular chaperones with roles in stabilizing and folding other proteins, heat shock protein 90 beta family member 1 (*Hsp90b1)* (Figure 2D and Supplementary Table 2).

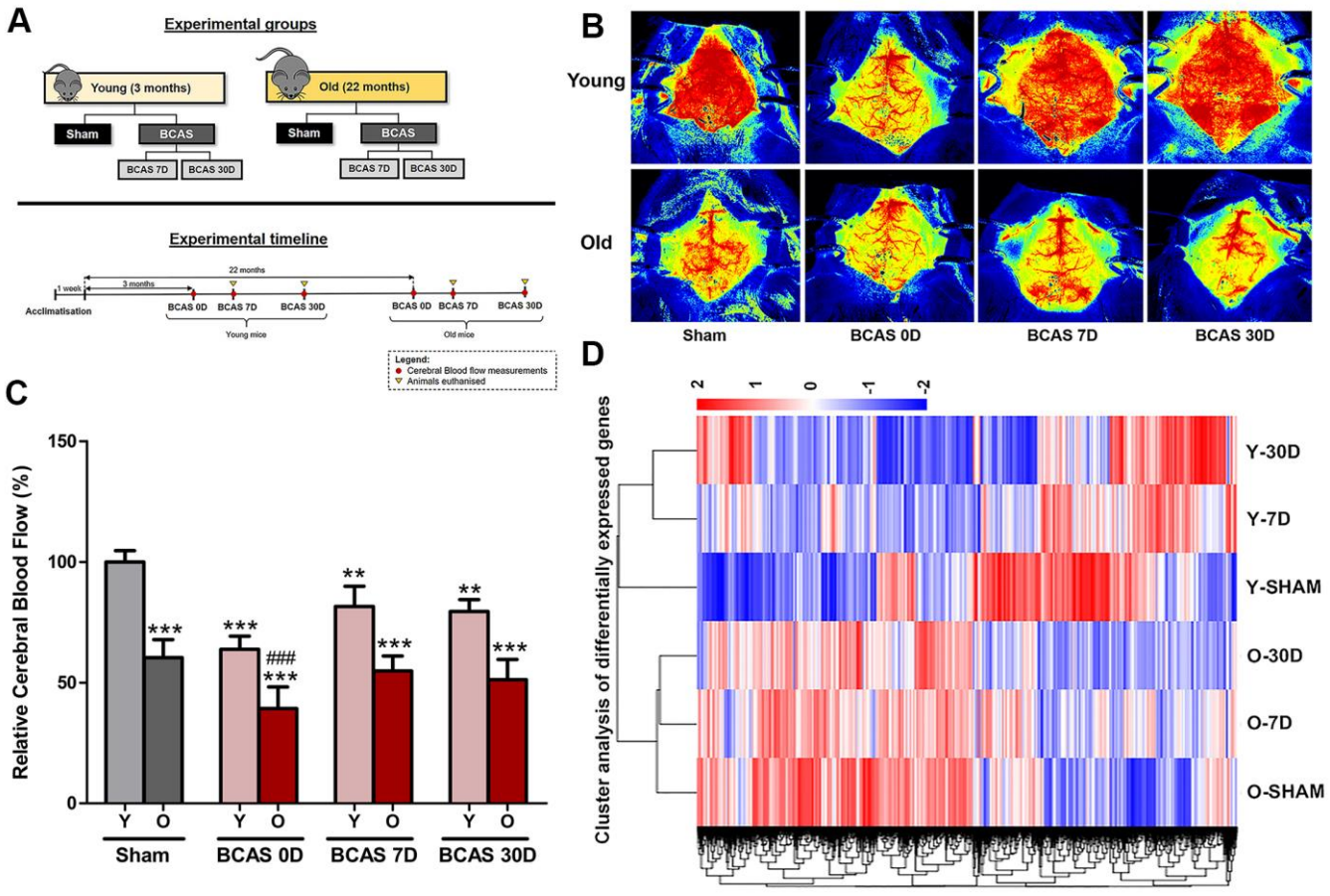

Figure 1. Effect of bilateral common carotid artery stenosis (BCAS) on cerebral blood flow and the respective gene expression profile in young and old mice. (**A**) Experimental model and timelines of blood flow measurements and tissue collection. Laser speckle contrasting imaging was used to monitor the cerebral blood perfusion in real time for all experimental groups before and after insertion of microcoils through BCAS surgery. (**B**, **C**) Representative contrast images and quantification of basal cerebral blood flow for young and old mice before surgery, and effective blood flow levels after 0, 7 and 30-days of BCAS (BCAS 0D, BCAS 7D and BCAS 30D respectively). The cerebral blood flow for the different experimental groups was compared to the normalised baseline (Y-Sham) and further comparisons within the different experimental groups were also performed. The relative cerebral blood flow data are presented in percentage upon calculation of the rate of blood flow in perfusion units (PU) (Refer to methods). Data are represented as mean ± S.E.M. n = 5 mice in each experimental group. **P<0.01 compared to Y-Sham; ***P<0.001 compared to Y-Sham; ###P<0.001 compared to O-Sham. (**D**) Heatmap of differentially expressed genes in Old Sham (OSham), Old 7 Day (O7D) BCAS, Old 30 Day (O30D) BCAS, Young Sham (YSham), Young 7 Day(Y7D) BCAS and Young 30 Day(Y30D) BCAS, groups with upregulated genes in red and downregulated genes in blue. The colour scale represents the log 10 (FPKM + 1) value.

Cerebral hypoperfusion

We assessed the effect of BCAS after 7 and 30 days on hippocampal gene expression in young and old mice. In young mice, there were global changes of gene expression patterns at both time points and significant DEGs that deviated from that of young sham-operated mice (Figure 3A). However, as for the reduction in CBF in old mice, BCAS did not result in profound changes in gene expression after either 7 or 30 days of BCAS compared to sham-operated old mice (Supplementary Figure 1). We thus focused our analyses on transcriptomic changes after BCAS in young mice. After 7 days, young mice had 279 significantly upregulated and 299 significantly downregulated genes compared to sham mice (Figure 3B), with more DEGs at 30 days than 7 days of BCAS. At 30 days, 598 genes were significantly upregulated and 552 genes were significantly downregulated in Y30D compared to sham mice (Figure 3B).

A full list of DEGs in the 7 and 30 days of BCAS groups is provided in Supplementary Table 3. The results of GO term analysis in young mice subjected to 7 days of BCAS revealed upregulation of genes involved in biological processes such as cell substrate junction, focal adhesion, myelin sheath, extracellular matrix, response to toxic substance, while biological processes such as ion channel complex, ion channel activity, transmembrane transporter complex, calcium channel activity, plasma membrane protein complex were significantly downregulated (Supplementary Figure 2). In addition to GO enrichment analysis, we performed Kyoto Encyclopedia of Genes and Genomes (KEGG) pathway enrichment analysis of the RNA sequencing data. Those results were generally similar to those of the GO term analysis, indicating pathways involved in focal adhesion, chemokine signaling pathway and long-term depression. KEGG analysis also revealed downregulation of gene sets related to calcium signaling, regulation of actin cytoskeleton, axon guidance, and memory (Supplementary Figure 3 and Supplementary Table 4).

The results of GO analysis revealed upregulation of genes involved in transcription factor activity, cofactor binding, mitochondrial inner membrane, organelle inner membrane, regulation of cellular amide metabolic process, cellular response to growth factor stimulus and reactive oxygen species metabolic process after 30 days of BCAS in young mice. GO terms such as regulation of cell morphogenesis, protein serine/threonine kinase activity, post-synaptic function and density, neurospine, excitatory synapse, dendritic spine, axon extension, ion

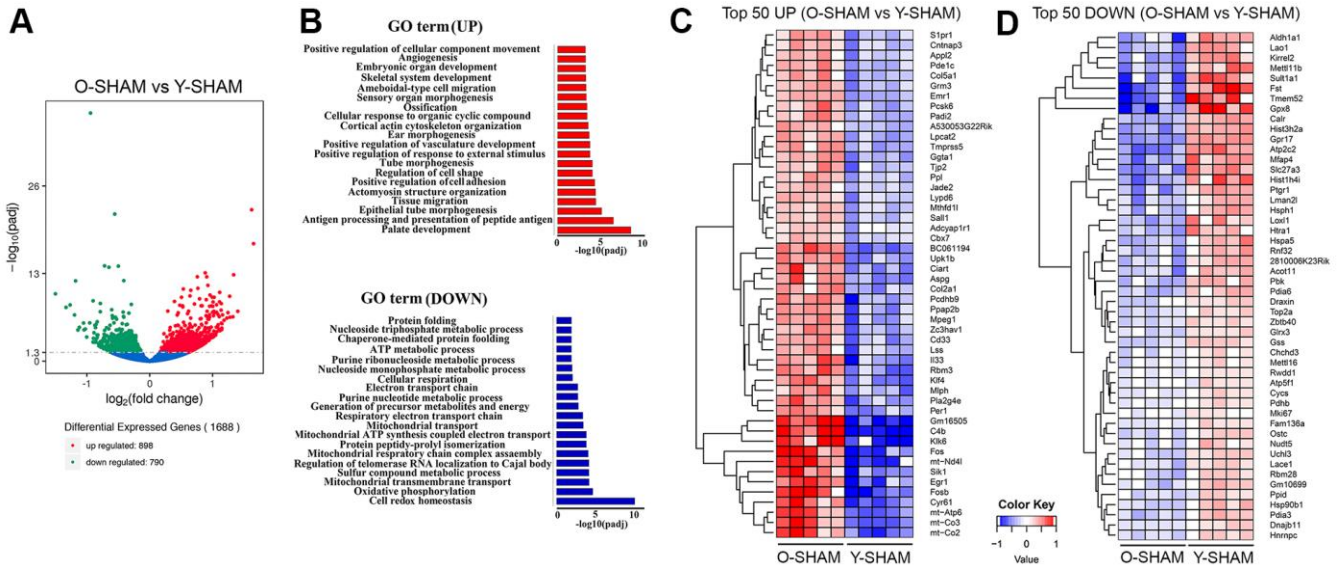

Figure 2. Analysis of differentially expressed genes in young and old hippocampus and their enriched GO terms. (**A**) Volcano plot of differentially expressed genes analyzed in old Sham group against young Sham group. The threshold of differential expression is q-value < 0.05. The horizontal axis is the log2 fold change of genes. The vertical axis is statistical significance scaled as -log 10 q-value. Each dot represents an individual gene (blue: no significant difference; red: upregulated expression of gene; green: down-regulated expression of gene). (**B**) The selection of significantly enriched top upregulated and down-regulated GO terms are presented for old Sham against young Sham animals (q < 0.05). The horizontal axis represents the -log10 scale for q-value of each GO term. (**C**) Top 50 up-regulated genes in old Sham against young Sham animals. (**D**) Top 50 down-regulated genes in old Sham against young Sham animals. Up-regulated genes in red and down-regulated genes in blue. The color scale represents the log10 (average FPKM+0.5) value.

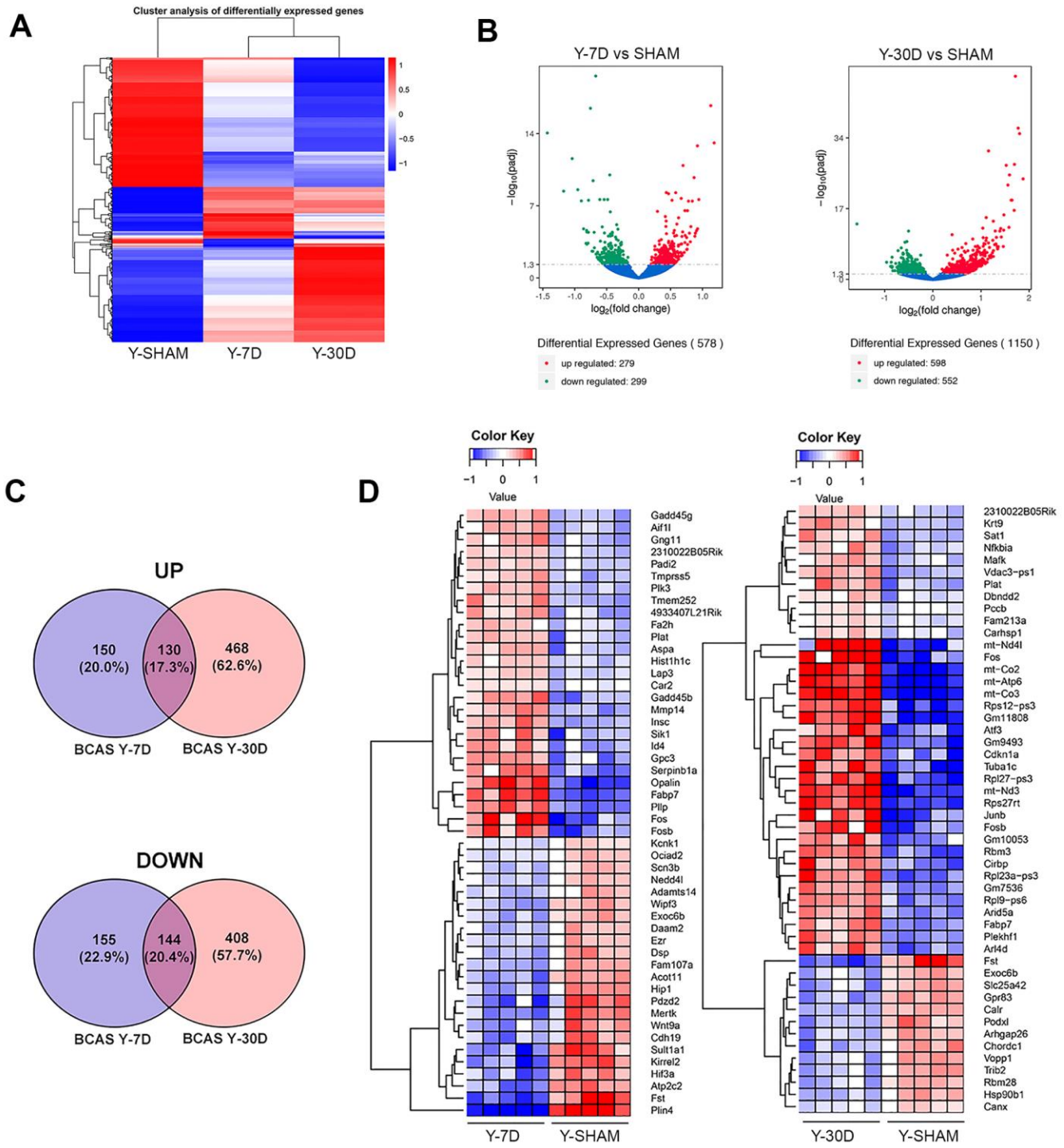

Figure 3. Differentially expressed genes in young hippocampus following chronic hypoperfusion. (**A**) Hierarchical clustering analysis of differentially expressed mRNA transcripts following 7 and 30 days BCAS compared to Sham animals. Upregulated genes in red and downregulated genes in blue. The color scale represents the log10 (average FPKM+1) value. (**B**) Volcano plots of differentially expressed genes analyzed in young 7 day and young 30 day BCAS animals compared to Sham animals. The threshold of differential expression is q value < 0.05. The horizontal axis is the log2 fold change of transcripts. The vertical axis is statistical significance scaled as -log 10 q-value. Each dot represents an individual transcript (blue: no significant difference; red: upregulated expression of gene; green: downregulated expression of gene). (**C**) Top 50 upregulated genes in young 7 day and young 30 day BCAS animals compared to Sham animals. (**D**) Venn diagram reflects the distribution of differentially expressed genes from 7 day and 30 day BCAS and Sham comparisons.

channel complex, phospholipid binding, transporter complex and transmembrane transporter complex were downregulated in these mice (Supplementary Figure 4 and Supplementary Table 5).

Temporal changes in DEGs during chronic cerebral hypoperfusion

The spread of unique DEGs after 7 or 30 days of BCAS in young mice were summarized in a Venn diagram (Figure 3C). There were some DEGs in common at 7 and 30 days, with 130 genes upregulated and 144 genes downregulated (Supplementary Table 6); however, there were approximately 3 times more DEGs in either direction at 30 versus 7 days (Figure 3C), consistent with a general temporal progression of hypoperfusion-induced injury at the transcriptome level (Figure 3C).

We narrowed our investigation to the top 50 DEGs at 7 and 30 days post-BCAS (Figure 3D). At 7 days, downregulated DEGs included a lipid marker of neurodegeneration transcript perilipin 4 (*Plin4*) [26], follistatin (*Fst*) [22], protein coding genes sulfotransferase family 1A member 1 (*Sult1a1*) and ATPase secretory pathway Ca^{2+} transporting 2 (*Atp2c2*), hypoxia inducible factor 3 subunit alpha (*Hif3a*), which acts as a transcriptional regulator in adaptive response to low oxygen tension [27] and myelin-forming cell-specific cadherin 19 (*Cdh19*) [28] among many other genes listed in Figure 3D. Upregulated DEGs included death promoting FosB proto-oncogene, AP-1 transcription factor subunit (*Fosb*) and Fos proto-oncogene, AP-1 transcription factor subunit (*Fos*) [29, 30], plasma membrane proteolipid (*Pllp*), and oligodendrocytic myelin paranodal and inner loop protein (*Opalin*) (Figure 3D).

At 30 days post-BCAS, downregulated DEGs included follistatin (*Fst*) [22], exocyst complex component 6B (*Exoc6b*), mitochondrial coenzyme A transporter (*Slc25a42*), stress response gene G Protein-Coupled Receptor 83 (*Gpr83*) [31], Ca^{2+}-binding chaperone protein Calreticulin (*Calr*) and neuroprotective heat shock protein 90kDa beta (*Grp94*) and member 1 (*Hsp90b1*) [32]. Upregulated DEGs included genes that were also upregulated in both old Sham mice and young mice at 7 days post-BCAS. These genes included: AP-1 transcription factor subunit (*Fos*), mitochondrially encoded cytochrome C oxidase III (*mt-Co3*), mitochondrially encoded cytochrome C oxidase II (*mt-Co2*), ATP synthase membrane subunit 6 (*Atp6*), mitochondrially encoded NADH:Ubiquinone oxidoreductase core subunit 3 (mt-nd3), cyclin dependent kinase inhibitor 1A (Cdkn1a), FosB proto-oncogene and AP-1 transcription factor subunit (*Fosb*) [29, 30] (Figure 3D).

Cerebral hypoperfusion and aging exhibit common changes in the hippocampal transcriptome

We assessed hippocampal transcriptome data from old sham-operated mice and young mice subjected to BCAS for 30 days in comparison with young sham-operated mice (Figure 4). The heatmap shows global changes of gene expression in these groups (Figure 4A). We found that over 4000 genes were differentially expressed between old sham-operated mice and young mice subjected to BCAS for 30 days with over 2300 genes downregulated (Figure 4A). The GO term analysis revealed that compared to BCAS-operated mice, old sham mice had downregulated biological processes mainly related to mitochondrial integrity (e.g. mitochondrial ribosome, mitochondrial inner membrane, mitochondrial protein complex, respiratory chain, mitochondrial matrix and NADH dehydrogenase complex) (Figure 4C). It is noteworthy that Venn diagram analyses indicated that old sham-operated mice and young mice subjected to BCAS for 30 days had in common 117 genes that were upregulated and 110 genes that were downregulated (Figure 4D, 4E). The common DEGs include those involved in the mitochondrial respiratory chain complex (Figure 4F) (e.g. mitochondrially encoded NADH dehydrogenase 3 and 4, *Mt-Nd3; Mt-Nd4*; mitochondrially encoded cytochrome c oxidase II and III, *Mt-Co2; Mt-Co3;* and mitochondrially Encoded ATP Synthase Membrane Subunit 6, *Mt-Atp6*. The 110 genes downregulated in both groups included mitochondrial genes (e.g. NADH:Ubiquinone Oxidoreductase Subunit B2 and NADH:Ubiquinone Oxidoreductase Complex Assembly Factor 4, *Ndufaf4*) (Figure 4F) and neuroprotective heat shock proteins (e.g. heat shock protein family H, *Hsp110;* member 1, *Hsph1;* heat shock protein family A, *Hsp70;* member 5, *Hspa5;* heat shock protein 90 alpha family class A member 1, *Hsp90aa1;* and heat shock protein 90 beta family member 1, *Hsp90b1*) (Figure 4G).

Our observation that aging and chronic cerebral hypoperfusion may both lead to hippocampal mitochondrial dysfunction and protein dysregulation led us to next validate our data by examining protein expression levels of selected genes (Figure 5). Immunoblot analysis confirmed that compared to young sham mice, mitochondrial proteins such as Mt-Atp6, Mt-Co2, Mt-Co3 were upregulated in old sham mice, while expression of Mt-Atp6 and Mt-Co2 tended to be higher in young mice subjected to 30 days of BCAS (Figure 5A). Neuroprotective protein chaperones such as GRP78 and Calnexin were downregulated following BCAS, while GRP78 was downregulated in old sham mice (Figure 5B).

To further examine the common pathways potentially altered in both aging and VaD pathology, we investigated the expression levels of PTEN-induced kinase 1 (Pink1) and E3 ubiquitin protein ligase PARKIN, two proteins which govern mitochondrial quality control [33]. Compared to young sham mice, hippocampal expression of both proteins was significantly higher after cerebral hypoperfusion for 30 days, and PARKIN was also higher in old sham mice (Figure 5C). We also validated two other proteins, Activin A and its antagonist follistatin (FST) [22], genes for which were differentially expressed in both

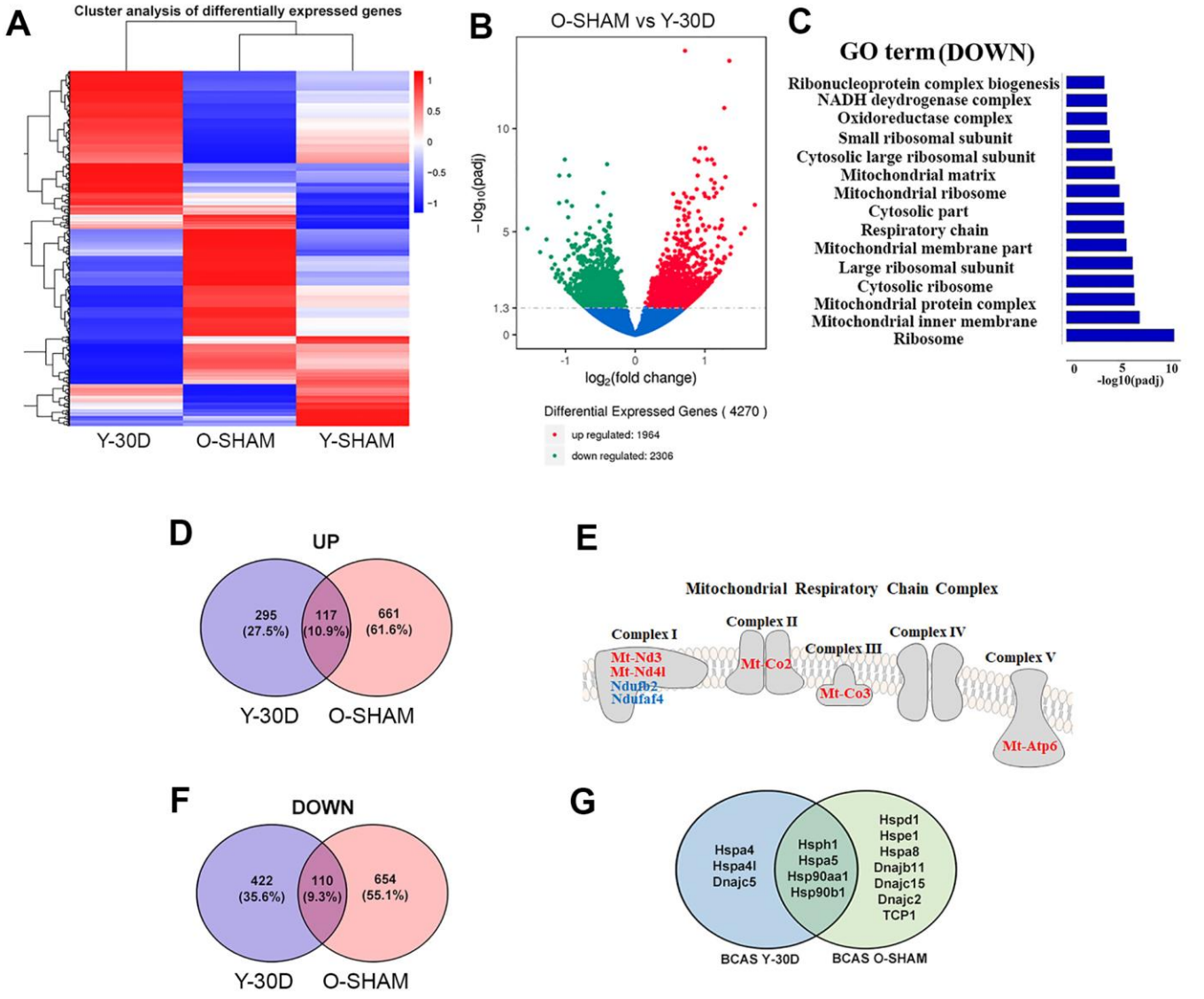

Figure 4. Comparative analyses of differentially expressed genes between young BCAS hippocampus and old Sham. (**A**) Hierarchical clustering analysis of differentially expressed genes following young 30 days BCAS and old Sham. Upregulated genes in red and down-regulated genes in blue. The color scale represents the log10 (average FPKM+1) value. (**B**) Differentially expressed mRNA transcripts analyzed between young 30 day BCAS and old Sham animals. The threshold of differential expression is q value < 0.05. The horizontal axis is the log2 fold change of transcripts. The vertical axis is statistical significance scaled as -log 10 q-value. Each dot represents an individual transcript (blue: no significant difference; red: upregulated transcript; green: down-regulated transcript). (**C**) The selection of significantly enriched down-regulated GO terms in both young 30 day BCAS and old Sham animals (q < 0.05). The horizontal axis represents the -log10 scale for q-value of each GO term. (**D**) Venn diagram reflects the distribution of differentially upregulated and downregulated genes from young 30-day BCAS and old Sham comparisons. (**E**) Venn diagram reflects the distribution of differentially down-regulated mRNA transcripts from young 30-day BCAS and old Sham comparisons. (**F**) Common upregulated (red) and downregulated (blue) mitochondrial genes in both young 30-day BCAS and old Sham hippocampus. (**G**) Common and unique down-regulated protein chaperons in young 30 day BCAS and old Sham groups.

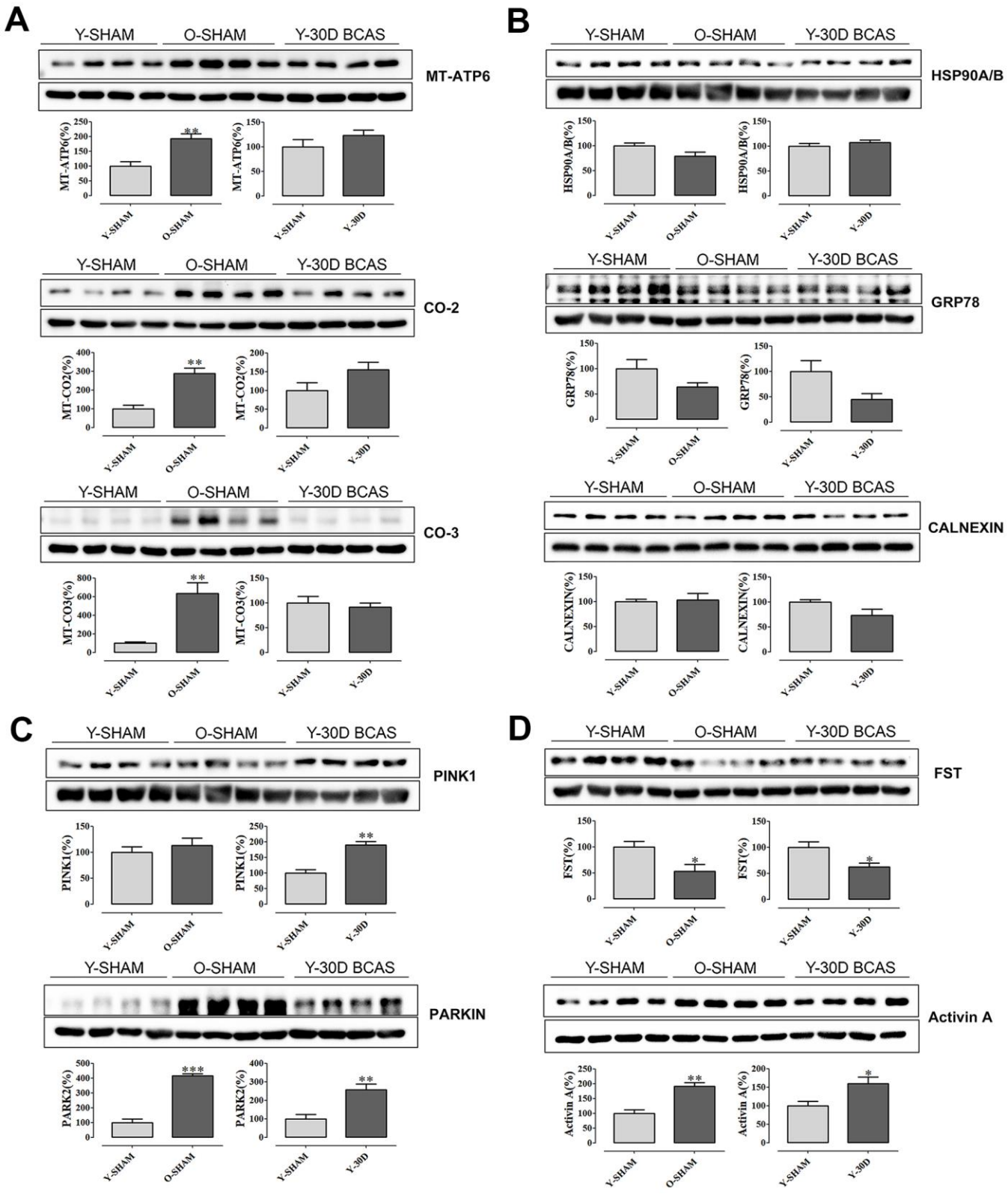

Figure 5. Immunoblot validation of mRNA transcripts. (**A**) Selected mitochondrial proteins Mt-Atp6, Mt-Co2, Mt-Co-3 and (**B**) protein chaperons Hsp90A/B, Grp78, Calnexin and (**C**) mitochondrial quality control proteins Park2 and Pink1 and (**D**) neuroprotective Activin A and its antagonist Fst. Data are represented as mean ± S.E.M. n=5-7 mice in each experimental group. *P<0.05 compared with young Sham; **P<0.01 compared with young Sham; ***P<0.001 compared with young Sham.

old sham mice and young mice following 30 days of BCAS. Our immunoblot data followed the patterns of gene expression, whereby FST was lower in these groups compared to young sham mice (Figure 5D). By contrast, Activin A expression was higher in these two treatment groups compared to young sham mice (Figure 5D).

Cell-type specific analyses

We next sorted the DEGs according to cell-type specificity based on previously published databases [34–37]. Relative to young sham mice, the cell-type specific profiles of significant DEGs are represented in six separate Venn diagrams according to the following: astrocytes, endothelial cells, microglia, neurons, oligodendrocytes and oligodendrocyte progenitor cells (OPCs) (Figure 6A). Protein-protein interaction (PPI) analyses revealed that most of the proteins associated with DEGs were independent of each other (Figure 6B–6E).

A similar analysis to identify age-associated cell-type specific genes that may promote disease pathology was then performed (Figure 7). DEGs were sorted according to cell-type specificity and visualized in Venn diagrams (Figure 7A). PPI analyses identified prominent interactions between old mice and those subjected to BCAS for 30 days in each cell type (Figure 7B–7G). While most proteins associated with DEGs were independent of each other in most cell types, the proteins associated with DEGs in the microglia of old sham mice had extensive interactions associated with proteins that promote neuroinflammation (Figure 7D).

To further investigate the overlap in DEGs between old mice and those subjected to BCAS for 30 days, the associated cell-type specific data were analyzed (Figure 8). All gene expression values were normalized using the average of the respective control in young sham mice. The overlapping cell-type specific common genes as identified in the Venn diagrams (Figure 7A) were Acyl-CoA Thioesterase 11 (*Acot11*) in astrocytes (Figure 8A), solute carrier family 38 member 5 (Slc38a5), solute Carrier Family 39 Member 8 (*Slc39a8*), protein coding gene Palmdelphin (*Palmd*) and apolipoprotein L Domain Containing 1 (*Apold1*) in endothelial cells (Figure 8B), lysophosphatidylcholine Acyltransferase 2 (*Lpcat2*) in microglia (Figure 8C), calcium voltage-gated channel auxiliary subunit alpha2delta 3 (Cacna2d3) in neurons (Figure 8D), arylsulfatase G (*Arsg*), aspartoacylase (*Aspa*), neurofascin (*Nfasc*), plasmolipin (*Pllp*), polypeptide N-acetylgalactosaminyltransferase 6 (*Galnt6*), INSC spindle orientation adaptor protein (*Insc*), oligodendrocytic myelin paranodal and inner loop protein (*Opalin*) and TNF alpha induced protein 6 (*Tnfaip6*) in oligodendrocytes (Figure 8E), S100 calcium binding protein B (*S100b*) and G protein-coupled receptor 17 (*Gpr17*) in OPCs (Figure 8F). While there was a general differential regulation of overlapping DEGs between old mice and those subjected to BCAS for 30 days across the different cell-types, it was notable that all but one of the DEGs classified under oligodendrocytes had relatively lower gene expression in old mice (Figure 8E). This cell-type specific analysis requires further validation to confirm the trends, but it serves as a starting point to identify overlaps between age- and disease-associated DEGs.

DISCUSSION

Chronic cerebral hypoperfusion causes progressive neurodegenerative disease that leads to cognitive decline in the elderly, and is increasingly being recognized as a major health issue. The hippocampus is central for human cognition, memory, executive function, intelligence, path integration and spatial processing [19], of which all functions decline with aging and reduced blood supply [38, 39]. Understanding how aging and the associated cerebral hypoperfusion may influence the hippocampal transcriptome may therefore identify mechanisms of impaired function and cognition. The present study is the first to investigate the impact of cerebral hypoperfusion and aging on the hippocampal transcriptome. The large datasets generated reveal progressive hippocampal transcriptomic responses during hypoperfusion, and somewhat similar changes with aging. Previous studies have demonstrated that cerebral hypoperfusion leads to white matter hyperintensities and brain atrophy via mechanisms such as energy imbalance, mitochondrial dysfunction, oxidative stress, neuroinflammation and neurovascular dysfunction [40]. This study has identified novel genes and signaling pathways in the hippocampus not previously implicated in this condition.

In order to ensure that cerebral hypoperfusion was present in mice subjected to BCAS, we measured CBF via laser speckle imaging. CBF reduction was consistently observed in the young and old mice immediately after the BCAS surgeries. In addition, partial recovery of CBF was over 7-30 days in young mice, consistent with the findings of Shibata and colleagues [14] our recent study [41]. We recently reported that in young mice, BCAS for 30 days produces features characteristic of VaD, including cognitive impairment, white matter lesions and neuronal loss in the hippocampal CA1, CA2 and CA3 regions [41]. By contrast, baseline CBF in old mice was lower than in young mice but returned to the pre-BCAS level

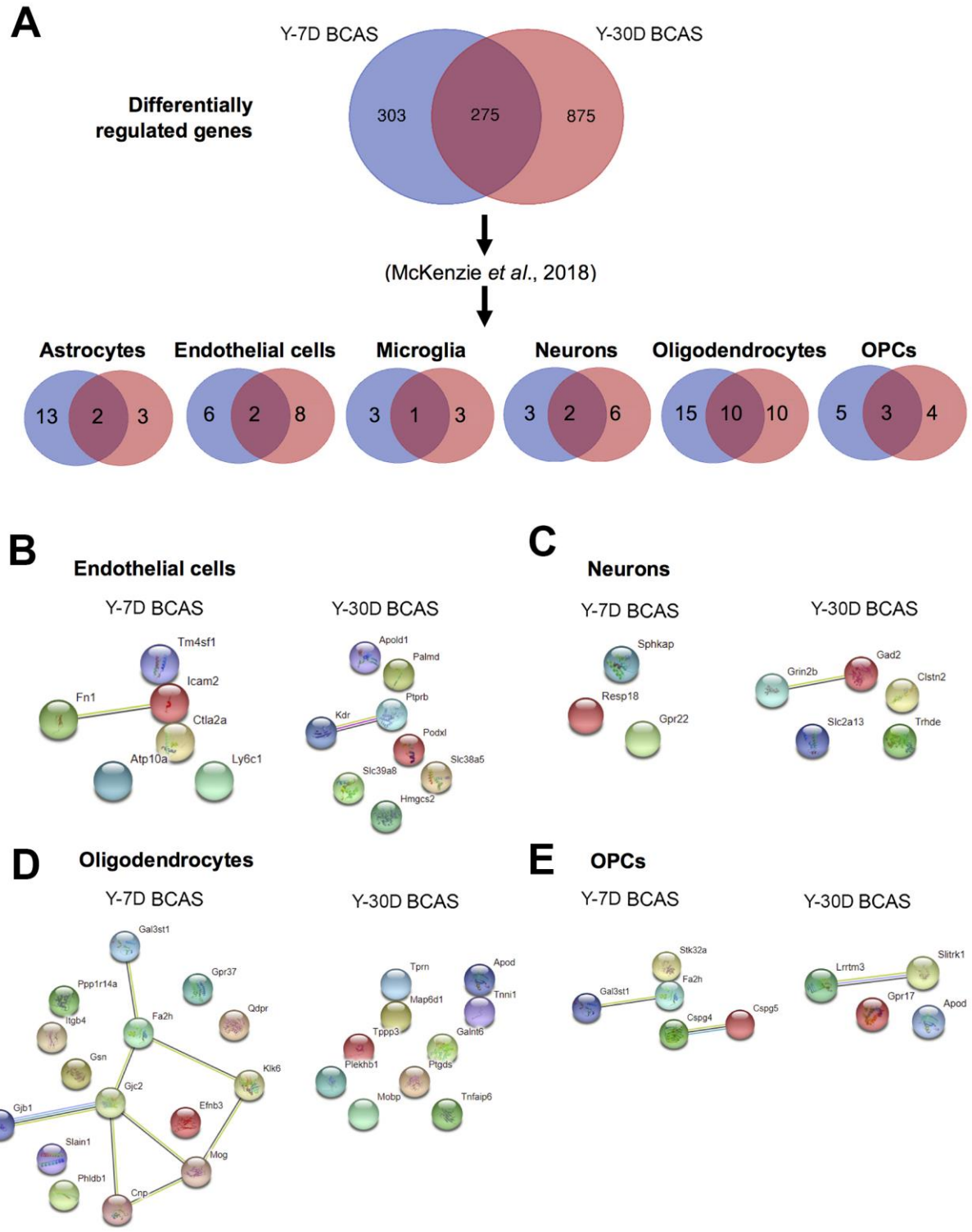

Figure 6. Analyses of differentially expressed mRNA transcripts in different brain cells following BCAS in young animals. (**A**) Venn diagram of statistically significant (adjusted p-value<0.05) differentially regulated genes in the Y7D/YSham vs Y30D/YSham comparison groups. The data was sorted according to cell type specificity based on a previously published database (Ref. 34) (Refer to Materials and Methods section for more details). The cell type specific profile of the genes are illustrated in six venn diagrams for each cell type including astrocytes, endothelial cells, microglia, neurons, oligodendrocytes and oligodendrocyte precursor cells (OPCs). The potential protein-protein interactions of cell type specific genes unique for the respective experimental groups of Y7D and Y30D respectively for endothelial cells (**B**), neurons (**C**), oligodendrocytes (**D**) and OPCs (**E**). The lines joining the different gene nodes indicate protein-protein associations such as known or predicted interactions and others such as text mining, co-expression or protein homology.

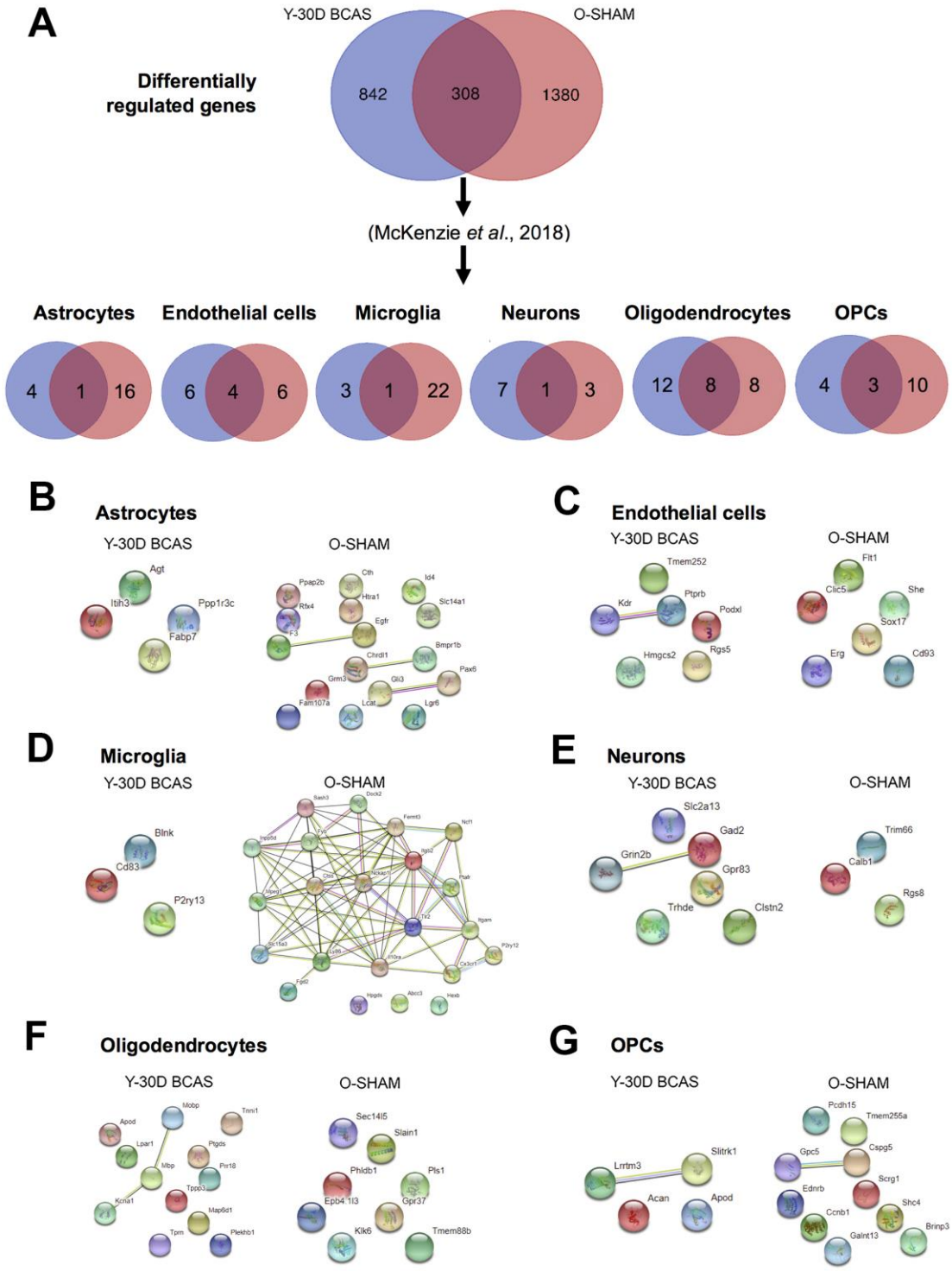

Figure 7. Analysis of differentially expressed mRNA transcripts in different brain cells in young 30 day BCAS animals compared to old Sham animals. (**A**) Venn diagram of statistically significant (adjusted p-value<0.05) differentially regulated genes in the Y30D/YSham vs OSham/YSham comparison groups. The data was sorted according to cell type specificity based on a previously published database (Ref. 34) (Refer to Materials and Methods section for more details). The cell type specific profile of the genes are illustrated in six venn diagrams for each cell type including astrocytes, endothelial cells, microglia, neurons, oligodendrocytes and oligodendrocyte precursor cells (OPCs). The potential protein-protein interactions of the cell type specific genes unique for the respective experimental groups of Y30D and OSham respectively for astrocytes (**B**), endothelial cells (**C**), microglia (**D**), neurons (**E**), oligodendrocytes (**F**) and OPCs (**G**). The lines joining the different gene nodes indicate protein-protein associations such as known or predicted interactions and others such as text mining, co-expression or protein homology.

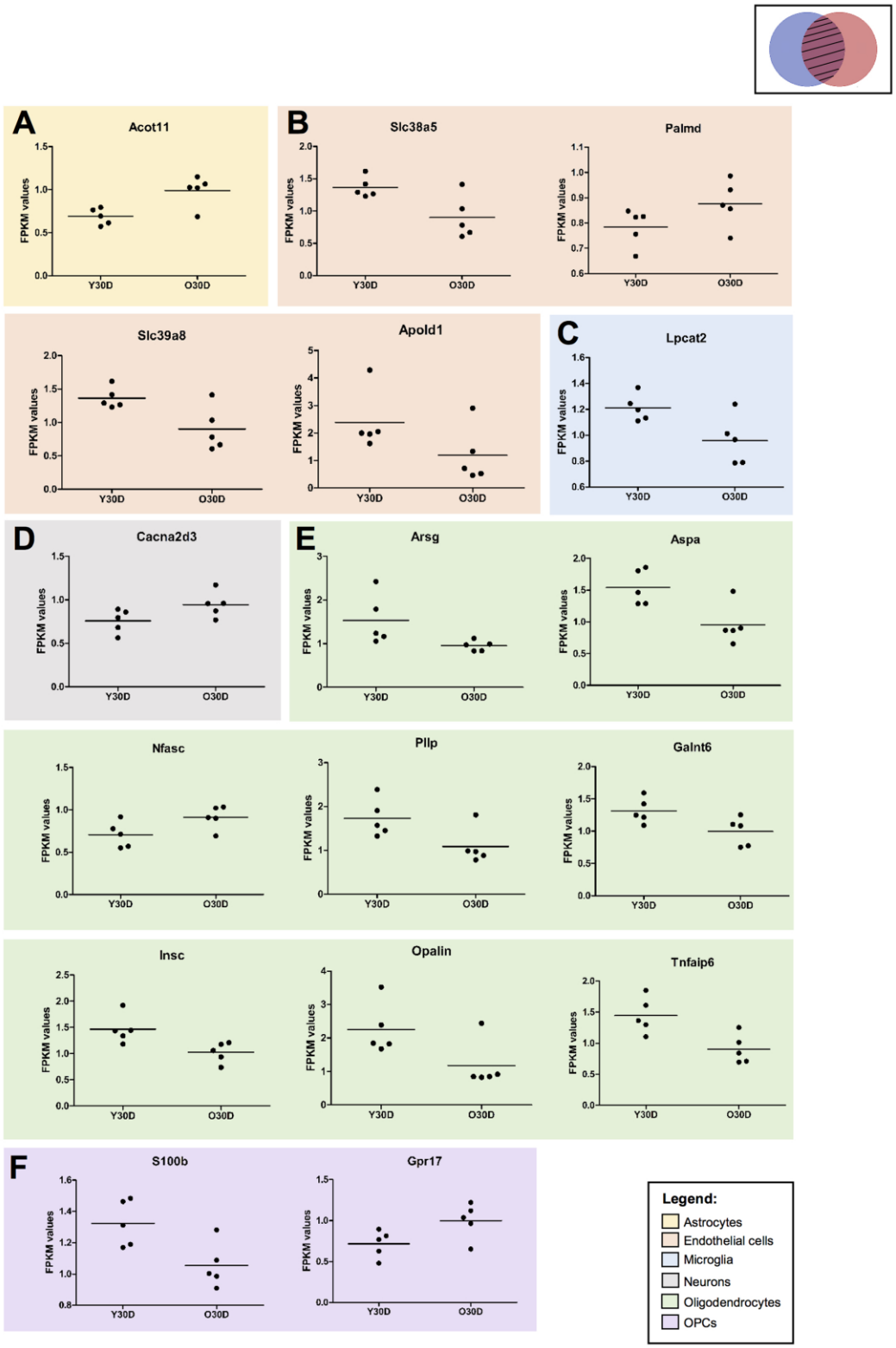

Figure 8. Expression of cell type specific genes overlapping between young 30-day BCAS and old Sham animals. (**A**) Astrocyte-associated gene (**B**) endothelial-associated genes (**C**) microglia-associated genes, (**D**) neuron-associated genes, (**E**) oligodendrocyte-associated genes, (**F**) OPC-associated genes. All gene expression values were normalised using the average of the respective controls (i.e. YSham for Y30D and OSham for O30D, respectively). Each dot corresponds to the biological replicates (n=5 for each group). The values are presented as FPKM values obtained through the RNA sequencing results. The solid horizontal lines represent the mean gene expression among the biological replicates.

by 7 days. Hence, the BCAS-induced CCH mouse model used in this study mimics the characteristic features observed in VaD patients, hence highlighting the validity of the model.

To further assess the effect of aging, we first examined transcriptomic differences between young (3-month old) and old (22-month-old) sham-operated mice. Consistent with a lower basal CBF in old versus young mice, transcriptomic data showed significant age-related differences in gene expression in the hippocampus. Numerous mitochondrial genes such as *mt-Atp6, mt-Co3, mt-Co2, mt-nd4l* were upregulated in old mice, potentially indicating impaired mitochondrial function. It was similarly reported that expression of other mitochondrial-encoded genes in complexes I, III, IV, and V of the respiratory chain was increased in the mouse brain during aging [42], and a recent study reported mt-Co2 expression to be increased in neuronal cells stimulated by α-Synuclein [43]. The α-Synuclein-induced decline in ATP levels, mitochondrial membrane potential and enhanced reactive oxygen species were reversed by inhibiting mt-Co2 gene expression, thus indicating that increased *mt-Co2* plays a detrimental role [43]. The most markedly upregulated DEG, as reflected by the distinct green dot with a high q-value in the volcano plot (Figure 2A) was noted to be aldehyde dehydrogenase 1 family member A1 (*Aldh1a1*) as per the heatmap (Figure 2D). Expression of *Aldh1a1*, whose role is implicated in neuronal patterns, differentiation and survival [44] is reportedly reduced in Parkinson's disease [45], perhaps also consistent with a possible disease-causing influence in old age also.

It is noteworthy that, compared with young sham mice, basal CBF was similarly reduced in old sham mice and in young mice subjected to cerebral hypoperfusion for 7 or 30 days. It is therefore plausible that a similar magnitude of chronic CBF reduction could account for overlaps between age- and disease-associated transcriptomic changes in the hippocampus, such as in differential expression of certain mitochondrial and oxidative genes. It is notable that the 7 and 30-day time points for BCAS surgery (i.e. the duration for which the microcoils are left in the mice) are selected to represent the early and late stage of the disease progression based on our optimization study [41]. This was based on the various pathological measures such as inflammasome activation, glial activation, cell death, white matter disruption and hippocampal neuronal density which were increased at 7 days and most pronounced at 30 days [41]. Thus, our findings show that relative to young sham mice, blood flow was already lower in old sham mice. Then, after BCAS blood flow is transiently reduced in the old mice and then returns to the pre-BCAS level - which is ~50% of blood flow young sham mice. This is in contrast to the post-BCAS blood flow in young mice which remains reduced relative to young sham blood flow levels. Therefore, unlike in young mice, it appears that old mice already exhibit evidence of chronic hypoperfusion at the level of blood flow such that microcoil-induced BCAS does not further substantially alter either blood flow or gene transcription

We have previously demonstrated that brain expression of cellular stress proteins such as *HSP70* and *GRP78* are greatly diminished in old mice [46]. Our transcriptomic data here similarly shows both aging and cerebral hypoperfusion result in downregulation of neuroprotective heat shock genes such as *Hsph1, Hspa5 (GRP78), Hsp90aa1* and *Hsp90b1*. All proteins encoded by these genes have been shown to protect neurons in multiple neurological conditions [47–49]. However, the specific signaling pathways and transcription factors that mediate downregulation of heat shock and other cellular stress proteins are yet to be identified. During aging, as expected, genes that promote cell death signals were significantly upregulated. Interestingly, this was also seen in young mice following cerebral hypoperfusion. Thus, upregulation of hippocampal genes involved in mitochondrial dysfunction and cell death, and downregulation of cellular protective genes could suggest a convergence of mechanisms resulting from the reduced cerebral blood supply during aging and BCAS. Given the current evidence, the young mice subjected to cerebral hypoperfusion show convergence in DEGs with the old sham mice, which is suggestive of possible accelerated aging. While further behavioural and histological experiments are required to validate this statement, another study validates our current finding. Wolf and colleagues had shown that young mice subjected to cerebral hypoperfusion and old sham mice were behaviorally analogous in exhibiting decreased social exploration and decreased velocity in open field that were not significantly different from each other [50].

GO term analyses of common downregulated DEGs in the hippocampus of both old and young mice after chronic cerebral hypoperfusion revealed additional ribosome-related genes that when altered may promote disease pathology, including ribonucloprotein complex biogenesis, small and large ribosomal subunits and ribosome. It is well established that loss of RNA homeostasis is a ubiquitous and central feature of neurodegenerative diseases [51]. It is noteworthy that telomerase is a ribonucleoprotein complex that maintains telomere length and known to play important roles in neural

stem progenitor cell proliferation, neuronal differentiation, survival and neurogenesis [52]. Understanding how cerebral hypoperfusion during aging affects telomerase expression and function will be an important area of future investigation. Ribosomal biogenesis is initiated in the nucleolus and includes the synthesis of ribosomal RNAs, assembly of ribosomal proteins, transportation to the cytoplasm and association of ribosomal subunits [53]. Disruption of ribosome biogenesis and decreased expression of small and large ribosomal subunits may promote cell cycle arrest, senescence or apoptosis [53, 54]. The relationship between downregulation of ribosomal genes and chronic hypoperfusion-induced brain pathology also requires further investigation.

The cell-type specific analyses, though preliminary, provide an avenue to identify clusters of proteins that play a role in age and disease-associated DEGs. With bioinformatics as a useful tool, this stratification is made possible and it provides a direction of focus for subsequent analyses. Evidence of microglial activation and endothelial dysfunction followed by BBB disruption have been established previously in VaD [1]. Hence, studying the different cell types would provide insights into the potential role they might play in driving the pathogenesis of cerebral hypoperfusion.

A limitation of this study that warrants future study is the lack of sex-specific analysis of the hippocampal transcriptome as only male mice were used here. Previous studies indicate that sex differences are likely to exist in the hippocampal transcriptome profile [55, 56]. Furthermore, as VaD is more prevalent in males than females [57], we postulate sex-specific alterations to be present but less profound in the context of this BCAS model.

In summary, this study has performed hippocampal transcriptomic profiling in both aging and chronic cerebral hypoperfusion that provided important findings. First, progressive transcriptomic changes are induced in both aging and following chronic cerebral hypoperfusion. Second, interestingly there is an overlap of DEGs and relevant disease pathways between aged and young mice subjected to chronic cerebral hypoperfusion. While limited to a 'landscape analysis', our results provide hypothesis-generating information that can be pursued in detail in future studies of hippocampal dysfunction in aging and models of age-related neurodegenerative diseases such as VaD. Indeed, elucidation of cell-specific pathological mechanisms common to aging and cerebral hypoperfusion should provide valuable insights for identifying therapeutic targets.

MATERIALS AND METHODS

Experimental animals and bilateral common carotid artery stenosis (BCAS) mouse model

All *in vivo* experimental procedures were approved by the National University of Singapore, Singapore Animal Care and Use Committee and performed according to the guidelines set forth by the National Advisory Committee for Laboratory Animal Research (NACLAR), Singapore. All experiments in the manuscript were performed and reported according to ARRIVE (Animal Research: Reporting *In Vivo* Experiments) guidelines.

Three-months old (Young animals; weighing 24 to 30 grams) and twenty-two months old (Old Animals; weighing 35 to 40 grams) male C57BL/6 mice were obtained from *In Vivos*, Singapore. Mice were housed in individual cages under standard laboratory conditions. Efforts were taken to minimise the number of animals used and to minimise their suffering during procedures. All mice had free access to food and water *ad libitum*. The experimental groups consist of 9-10 mice in each group. Animals were anaesthetized with isoflurane and subjected to BCAS. BCAS involved using microcoils specially designed for the mice (microcoil specifications: piano wire diameter 0.08mm, internal diameter 0.18mm, coiling pitch 0.5mm, and total length 2.5mm; Sawane Spring Co Ltd, Japan). BCAS was performed by exposing the left and right common carotid arteries (CCAs) one-by-one, freed from their sheaths, and twining a microcoil by rotating it around each CCA. Sham surgeries were performed as controls where the site of surgery was opened and the CCAs were gently touched using the forceps without insertion of microcoils. The site of surgery was subsequently closed using surgical glue, and the mice were observed and taken care of post-surgery until conscious and recovered to freely access food and water *ad libitum*. All animals were euthanized via inhalation of carbon dioxide gas at their respective end-points after BCAS for subsequent analysis.

Measurements of cerebral blood flow by laser speckle contrast imager

High-resolution Laser Speckle Contrast Imager (PSI system, Perimed Inc.) was used to image cerebral blood perfusion and record cerebral blood flow (CBF) before insertion of the microcoils (baseline), immediately after the insertion of the microcoils and finally at their respective end-points of BCAS. Body temperature of the mice was maintained at 37 ± 0.5° C. The skull of the mice were shaved and exposed by a midline skin incision. The skull was cleaned gently with sterile

phosphate buffered saline (PBS) using a cotton applicator. The image area was kept moist and a non-toxic silicon oil was applied on the skull, improving the imaging. Perfusion images were acquired using the PSI system with a 70 mW built-in laser diode for illumination and a 1388 x 1038 pixels CCD camera installed 10 cm above the skull (speed 19 Hz, and exposure time 6 mSec). Analyses of CBF changes were done on the acquired images using a dedicated PIMSoft program (Perimed Inc.).

Sample collection and processing

At the end of each BCAS time point or sham surgeries, the mice were euthanized by administering a lethal dose of carbon dioxide (CO_2) for inhalation and the brains were harvested. The hippocampi were immediately separated on ice and were stored in a -80^{o}C freezer for RNA sequencing analysis (n = 5 in each experimental group). A separate group of animals were sacrificed for immunoblot analysis (n = 4-5 in each experimental group).

Total RNA extraction and validation

Total RNA were extracted from frozen brain tissue samples using a micro-tube tissue homogenizer (Bel-Art, Wayne, NJ, USA) and EZ-10 DNAaway RNA extraction mini-prep kit (Bio Basic, Ontario, Canada) following manufacturer's instructions. Assessment of the integrity and quality of extracted total RNA was performed using agarose gel electrophoresis and Agilent 2100 Bioanalyser (Agilent, Santa Clara, CA, USA); all RNA samples showed RNA integrity numbers above 7, indicating high quality of the extracted total RNA.

cDNA library preparation and RNA sequencing

The mRNA was purified from total RNA using poly-T oligo-attached magnetic beads and was first fragmented randomly by addition of fragmentation buffer. Subsequently, the first-strand of cDNA was synthesized using a random hexamer primer and M-MuLV reverse transcriptase (RNase H-) (New England BioLabs, Ipswish, MA, USA). Next, DNA polymerase I and RNase H were used to synthesize the second strand. Double-stranded cDNA was purified using AMPure XP beads (Beckman Courter Life Sciences, Indianapolis, IN, USA). Remaining overhangs of the purified double-stranded cDNA were converted into blunt ends via exonuclease/polymerase activities. After adenylation of 3'-ends of DNA fragments, NEBNext adaptor with hairpin loop structure was ligated to prepare for hybridization. In order to select cDNA fragments of preferentially 150-200bp in length, the library fragments were purified with AMPure XP system. Finally, the library was acquired by polymerase chain reaction (PCR) amplification and purification of PCR products by AMPure XP beads. High-throughput sequencing was conducted using HiSeqTM2500 platform (Illumina, San Diego, CA, USA).

Transcriptome data mapping and differential expression analysis

The RNA sequencing results from the HiSeq system were generated as fasta and quality files, and these files were mapped to the Ensembl-released mouse genome sequence and annotation. Indexes of the reference genome were built using Bowtie V.2.0.6 and paired-end clean reads were aligned to the reference genome using TopHat V.2.0.9 with mismatch parameter limited to 2. For the quantification of gene expression level, HTSeq V.0.6.1 was used to count the read numbers mapped of each gene. Then Reads Per Kilobase of exon model per Million mapped reads (RPKM) of each gene was calculated based on the length of the gene and reads count mapped to the same gene. Differential expression analysis was performed using the DESeq R Package V.1.10.1 and the resulting P-values were adjusted using the Benjamini and Hochberg's approach for controlling the FDR. Genes with an adjusted P-value lower than 0.05 found by DESeq were assigned as differentially expressed.

Heatmap generation and enrichment analyses

To create heat maps of differentially expressed genes (DEGs), the R package heatmap3 were used along with the log2Fold-Change output from EdgeR V.3.2.4. To assess the biological significance of gene expression changes, GO and KEGG pathway enrichment analyses were conducted. GO enrichment analysis, focused on biological processes of differentially expressed genes was implemented by the GOseq R package in which gene length bias was corrected. For KEGG pathway enrichment analysis, we used KEGG Orthology-Based Annotation System (KOBAS) software to test the statistical enrichment. GO terms or KEGG pathways with adjusted P-value less than 0.05 were considered significantly enriched by differentially expressed genes.

Sorting based on cell-type specificity

McKenzie and colleagues [34] had compared murine cell-type specific transcriptome-wide RNA expression data sets from three different groups [35–37]. Out of the three mice databases, the top 1000 genes per cell type were selected and ranked according to three cell type associated measures. These include (i) cell-type enrichment which compares if a gene tends to have a higher expression in one cell type compared to the

others, (ii) cell-type expression where it compares whether a gene is expressed in a given cell type irrespective of expression levels in the other cell types and (iii) specificity where it compares whether a gene is expressed in only one cell type. Based on the aim of this project, the 1000 genes per cell type were further filtered to the top 100 genes based on specificity and cell enrichment in its respective order.

Immunoblot analysis

Brain tissues were homogenized in lysis buffer and then combined with 2 x Laemelli buffer (Bio-Rad Laboratories, Inc., Hercules, CA, USA). Protein samples were then separated on 7.5 to 12.5% v/v sodium dodecyl sulfate (SDS) gels. The SDS-PAGE gels were transferred onto nitrocellulose membranes to probe for proteins. Next, the nitrocellulose membranes were incubated with the following primary antibodies: Mt-ATP6 (Santa Cruz Biotechnology, sc-81886), COX2 (Santa Cruz Biotechnology, sc-514489), COX3 (Santa Cruz Biotechnology, sc-23986), HSP90 (Santa Cruz Biotechnology, sc-13119), GRP78 (Santa Cruz Biotechnology, sc-13539), Calnexin (Santa Cruz Biotechnology, sc-23954), Pink1 (Santa Cruz Biotechnology, sc-517353), PRK8 (Santa Cruz Biotechnology, sc-32282), Fst (Santa Cruz Biotechnology, sc-365003), ActivinA (Novus, NBP1-30928) and β-actin (Sigma-Aldrich, A5441) overnight at 4° C with agitation. Following primary antibody incubation, membranes were washed three times with 1xTBST before incubating with horseradish peroxidase (HRP)-conjugated secondary antibodies (Goat Anti-Rabbit – Cell Signaling Technology, Danvers, MA, USA; Goat Anti-Mouse – Sigma-Aldrich, St. Louis, MO, USA; Goat Anti-Rat – GE Healthcare Life Sciences, Little Chalfont, UK) for 1 hr at 24° C with agitation. Following secondary antibody incubation, membranes were washed three times with 1xTBST, each time for 10min. The substrate for HRP, enhanced chemiluminescence (ECL) (Bio-Rad Laboratories, Inc., Hercules, CA, USA) was applied before the membranes were imaged using the ChemiDocXRS+imaging system (Bio-Rad Laboratories, Inc., Hercules, CA, USA). Quantification of proteins was conducted using Image J software (Version 1.46; National Institute of Health, Bethesda, MD, USA), where protein densitometry was expressed relative to the densitometry of the corresponding β-actin.

Authors' note

High-throughput sequencing data from this manuscript have been submitted to the NCBI Sequence Read Archive (SRA) and accession number will be available. Data are however available from the corresponding authors (Arumugam or Sobey) upon reasonable request. The authors thank the Novogene (Beijing, China) for kind assistance in data processing.

AUTHOR CONTRIBUTIONS

Study Conception and Design: T.V.A., S.H.B., D.G.J., D.R.H., M.K.P.L., C.L.H.C., G.R.D., K.L.L., and C.G.S; Investigation-Performed Experiment or Data Collection: T.V.A., S.H.B., D.Y.F., L.P., and S.S., Data Analysis: S.H.B., S.S., and T.V.A.; Data Interpretation: S.H.B., S.S., and T.V.A.; Writing-Manuscript Preparation and intellectual input: T.V.A., S.H.B., S.S., D.G.J., D.R.H., S.R.Z., H.A.K., T.M.D.S., M.K.P.L., C.L.H.C., G.R.D., K.L.L., and C.G.S; Supervision and Administration: T.V.A., and C.L.H.C.

CONFLICTS OF INTEREST

The authors declare that they have no conflicts of interest.

FUNDING

This work was supported by the National University of Singapore, Singapore National Medical Research Council Research Grants (NMRC-CBRG-0102/2016 and NMRC/OFIRG/0036/2017), Singapore Ministry of Education (MOE2017-T3-1-002) and La Trobe University, Australia.

REFERENCES

1. Venkat P, Chopp M, Chen J. Models and mechanisms of vascular dementia. Exp Neurol. 2015; 272:97–108. https://doi.org/10.1016/j.expneurol.2015.05.006 PMID:25987538

2. Knopman DS, Rocca WA, Cha RH, Edland SD, Kokmen E. Survival study of vascular dementia in Rochester, Minnesota. Arch Neurol. 2003; 60:85–90. https://doi.org/10.1001/archneur.60.1.85 PMID:12533093

3. Rizzi L, Rosset I, Roriz-Cruz M. Global epidemiology of dementia: Alzheimer's and vascular types. Biomed Res Int. 2014; 2014:908915. https://doi.org/10.1155/2014/908915 PMID:25089278

4. Wolters FJ, Ikram MA. Epidemiology of Vascular Dementia. Arterioscler Thromb Vasc Biol. 2019; 39:1542–49. https://doi.org/10.1161/ATVBAHA.119.311908 PMID:31294622

5. Gorelick PB, Scuteri A, Black SE, Decarli C, Greenberg SM, Iadecola C, Launer LJ, Laurent S, Lopez OL, Nyenhuis D, Petersen RC, Schneider JA, Tzourio C, et al,

and American Heart Association Stroke Council, Council on Epidemiology and Prevention, Council on Cardiovascular Nursing, Council on Cardiovascular Radiology and Intervention, and Council on Cardiovascular Surgery and Anesthesia. Vascular contributions to cognitive impairment and dementia: a statement for healthcare professionals from the American heart association/American stroke association. Stroke. 2011; 42:2672–713. https://doi.org/10.1161/STR.0b013e3182299496 PMID:21778438

6. van der Flier WM, Skoog I, Schneider JA, Pantoni L, Mok V, Chen CL, Scheltens P. Vascular cognitive impairment. Nat Rev Dis Primers. 2018; 4:18003. https://doi.org/10.1038/nrdp.2018.3 PMID:29446769

7. Parkes I, Chintawar S, Cader MZ. Neurovascular dysfunction in dementia - human cellular models and molecular mechanisms. Clin Sci (Lond). 2018; 132:399–418. https://doi.org/10.1042/CS20160720 PMID:29444850

8. Iadecola C, Duering M, Hachinski V, Joutel A, Pendlebury ST, Schneider JA, Dichgans M. Vascular Cognitive Impairment and Dementia: JACC Scientific Expert Panel. J Am Coll Cardiol. 2019; 73:3326–44. https://doi.org/10.1016/j.jacc.2019.04.034 PMID:31248555

9. van Veluw SJ, Hilal S, Kuijf HJ, Ikram MK, Xin X, Yeow TB, Venketasubramanian N, Biessels GJ, Chen C. Cortical microinfarcts on 3T MRI: Clinical correlates in memory-clinic patients. Alzheimers Dement. 2015; 11:1500–09. https://doi.org/10.1016/j.jalz.2014.12.010 PMID:25956990

10. Hilal S, Sikking E, Shaik MA, Chan QL, van Veluw SJ, Vrooman H, Cheng CY, Sabanayagam C, Cheung CY, Wong TY, Venketasubramanian N, Biessels GJ, Chen C, Ikram MK. Cortical cerebral microinfarcts on 3T MRI: A novel marker of cerebrovascular disease. Neurology. 2016; 87:1583–90. https://doi.org/10.1212/WNL.0000000000003110 PMID:27590296

11. Hilal S, Chai YL, van Veluw S, Shaik MA, Ikram MK, Venketasubramanian N, Richards AM, Biessels GJ, Chen C. Association Between Subclinical Cardiac Biomarkers and Clinically Manifest Cardiac Diseases With Cortical Cerebral Microinfarcts. JAMA Neurol. 2017; 74:403–10. https://doi.org/10.1001/jamaneurol.2016.5335 PMID:28166312

12. Ferro DA, Mutsaerts HJ, Hilal S, Kuijf HJ, Petersen ET, Petr J, van Veluw SJ, Venketasubramanian N, Yeow TB, Biessels GJ, Chen C. Cortical microinfarcts in memory clinic patients are associated with reduced cerebral perfusion. J Cereb Blood Flow Metab. 2020; 40:1869–78. https://doi.org/10.1177/0271678X19877403 PMID:31558107

13. Washida K, Hattori Y, Ihara M. Animal Models of Chronic Cerebral Hypoperfusion: From Mouse to Primate. Int J Mol Sci. 2019; 20:6176. https://doi.org/10.3390/ijms20246176 PMID:31817864

14. Shibata M, Ohtani R, Ihara M, Tomimoto H. White matter lesions and glial activation in a novel mouse model of chronic cerebral hypoperfusion. Stroke. 2004; 35:2598–603. https://doi.org/10.1161/01.STR.0000143725.19053.60 PMID:15472111

15. Bink DI, Ritz K, Aronica E, van der Weerd L, Daemen MJ. Mouse models to study the effect of cardiovascular risk factors on brain structure and cognition. J Cereb Blood Flow Metab. 2013; 33:1666–84. https://doi.org/10.1038/jcbfm.2013.140 PMID:23963364

16. Ihara M, Taguchi A, Maki T, Washida K, Tomimoto H. A mouse model of chronic cerebral hypoperfusion characterizing features of vascular cognitive impairment. Methods Mol Biol. 2014; 1135:95–102. https://doi.org/10.1007/978-1-4939-0320-7_8 PMID:24510857

17. Shibata M, Yamasaki N, Miyakawa T, Kalaria RN, Fujita Y, Ohtani R, Ihara M, Takahashi R, Tomimoto H. Selective impairment of working memory in a mouse model of chronic cerebral hypoperfusion. Stroke. 2007; 38:2826–32. https://doi.org/10.1161/STROKEAHA.107.490151 PMID:17761909

18. O'Shea A, Cohen RA, Porges EC, Nissim NR, Woods AJ. Cognitive Aging and the Hippocampus in Older Adults. Front Aging Neurosci. 2016; 8:298. https://doi.org/10.3389/fnagi.2016.00298 PMID:28008314

19. Hattori Y, Enmi J, Iguchi S, Saito S, Yamamoto Y, Nagatsuka K, Iida H, Ihara M. Substantial Reduction of Parenchymal Cerebral Blood Flow in Mice with Bilateral Common Carotid Artery Stenosis. Sci Rep. 2016; 6:32179. https://doi.org/10.1038/srep32179 PMID:27535801

20. Raivich G, Behrens A. Role of the AP-1 transcription factor c-Jun in developing, adult and injured brain. Prog Neurobiol. 2006; 78:347–63. https://doi.org/10.1016/j.pneurobio.2006.03.006 PMID:16716487

21. Gao C, Du Q, Li W, Deng R, Wang Q, Xu A, Shen J. Baicalin Modulates APPL2/Glucocorticoid Receptor Signaling Cascade, Promotes Neurogenesis, and Attenuates Emotional and Olfactory Dysfunctions in Chronic Corticosterone-Induced Depression. Mol Neurobiol. 2018; 55:9334–48. https://doi.org/10.1007/s12035-018-1042-8 PMID:29675572

22. Tretter YP, Hertel M, Munz B, ten Bruggencate G, Werner S, Alzheimer C. Induction of activin A is essential for the neuroprotective action of basic fibroblast growth factor *in vivo*. Nat Med. 2000; 6:812–15. https://doi.org/10.1038/77548 PMID:10888932

23. Ramming T, Hansen HG, Nagata K, Ellgaard L, Appenzeller-Herzog C. GPx8 peroxidase prevents leakage of H2O2 from the endoplasmic reticulum. Free Radic Biol Med. 2014; 70:106–16. https://doi.org/10.1016/j.freeradbiomed.2014.01.018 PMID:24566470

24. Sánchez-Rodríguez R, Torres-Mena JE, Quintanar-Jurado V, Chagoya-Hazas V, Rojas Del Castillo E, Del Pozo Yauner L, Villa-Treviño S, Pérez-Carreón JI. Ptgr1 expression is regulated by NRF2 in rat hepatocarcinogenesis and promotes cell proliferation and resistance to oxidative stress. Free Radic Biol Med. 2017; 102:87–99. https://doi.org/10.1016/j.freeradbiomed.2016.11.027 PMID:27867096

25. Newbury DF, Winchester L, Addis L, Paracchini S, Buckingham LL, Clark A, Cohen W, Cowie H, Dworzynski K, Everitt A, Goodyer IM, Hennessy E, Kindley AD, et al. CMIP and ATP2C2 modulate phonological short-term memory in language impairment. Am J Hum Genet. 2009; 85:264–72. https://doi.org/10.1016/j.ajhg.2009.07.004 PMID:19646677

26. Chali F, Milior G, Marty S, Morin-Brureau M, Le Duigou C, Savary E, Blugeon C, Jourdren L, Miles R. Lipid markers and related transcripts during excitotoxic neurodegeneration in kainate-treated mice. Eur J Neurosci. 2019; 50:1759–78. https://doi.org/10.1111/ejn.14375 PMID:30767299

27. Heidbreder M, Fröhlich F, Jöhren O, Dendorfer A, Qadri F, Dominiak P. Hypoxia rapidly activates HIF-3alpha mRNA expression. FASEB J. 2003; 17:1541–43. https://doi.org/10.1096/fj.02-0963fje PMID:12824304

28. Zorniak M, Clark PA, Kuo JS. Myelin-forming cell-specific cadherin-19 is a marker for minimally infiltrative glioblastoma stem-like cells. J Neurosurg. 2015; 122:69–77. https://doi.org/10.3171/2014.9.JNS132373 PMID:25361488

29. McGahan L, Hakim AM, Nakabeppu Y, Robertson GS. Ischemia-induced CA1 neuronal death is preceded by elevated FosB and Jun expression and reduced NGFI-A and JunB levels. Brain Res Mol Brain Res. 1998; 56:146–61. https://doi.org/10.1016/s0169-328x(98)00039-4 PMID:9602101

30. Hughes PE, Alexi T, Walton M, Williams CE, Dragunow M, Clark RG, Gluckman PD. Activity and injury-dependent expression of inducible transcription factors, growth factors and apoptosis-related genes within the central nervous system. Prog Neurobiol. 1999; 57:421–50. https://doi.org/10.1016/s0301-0082(98)00057-4 PMID:10080384

31. Lueptow LM, Devi LA, Fakira AK. Targeting the Recently Deorphanized Receptor GPR83 for the Treatment of Immunological, Neuroendocrine and Neuropsychiatric Disorders. Prog Mol Biol Transl Sci. 2018; 159:1–25. https://doi.org/10.1016/bs.pmbts.2018.07.002 PMID:30340784

32. Cheng Y, Yang C, Zhao J, Tse HF, Rong J. Proteomic identification of calcium-binding chaperone calreticulin as a potential mediator for the neuroprotective and neuritogenic activities of fruit-derived glycoside amygdalin. J Nutr Biochem. 2015; 26:146–54. https://doi.org/10.1016/j.jnutbio.2014.09.012 PMID:25465157

33. Pickrell AM, Youle RJ. The roles of PINK1, parkin, and mitochondrial fidelity in Parkinson's disease. Neuron. 2015; 85:257–73. https://doi.org/10.1016/j.neuron.2014.12.007 PMID:25611507

34. McKenzie AT, Wang M, Hauberg ME, Fullard JF, Kozlenkov A, Keenan A, Hurd YL, Dracheva S, Casaccia P, Roussos P, Zhang B. Brain Cell Type Specific Gene Expression and Co-expression Network Architectures. Sci Rep. 2018; 8:8868. https://doi.org/10.1038/s41598-018-27293-5 PMID:29892006

35. Tasic B, Menon V, Nguyen TN, Kim TK, Jarsky T, Yao Z, Levi B, Gray LT, Sorensen SA, Dolbeare T, Bertagnolli D, Goldy J, Shapovalova N, et al. Adult mouse cortical cell taxonomy revealed by single cell transcriptomics. Nat Neurosci. 2016; 19:335–46. https://doi.org/10.1038/nn.4216 PMID:26727548

36. Zeisel A, Muñoz-Manchado AB, Codeluppi S, Lönnerberg P, La Manno G, Juréus A, Marques S, Munguba H, He L, Betsholtz C, Rolny C, Castelo-Branco G, Hjerling-Leffler J, Linnarsson S. Brain structure. Cell types in the mouse cortex and hippocampus revealed by single-cell RNA-seq. Science. 2015; 347:1138–42.

https://doi.org/10.1126/science.aaa1934
PMID:25700174

37. Zhang Y, Sloan SA, Clarke LE, Caneda C, Plaza CA, Blumenthal PD, Vogel H, Steinberg GK, Edwards MS, Li G, Duncan JA 3rd, Cheshier SH, Shuer LM, et al. Purification and Characterization of Progenitor and Mature Human Astrocytes Reveals Transcriptional and Functional Differences with Mouse. Neuron. 2016; 89:37–53.
https://doi.org/10.1016/j.neuron.2015.11.013
PMID:26687838

38. Bettio LE, Rajendran L, Gil-Mohapel J. The effects of aging in the hippocampus and cognitive decline. Neurosci Biobehav Rev. 2017; 79:66–86.
https://doi.org/10.1016/j.neubiorev.2017.04.030
PMID:28476525

39. Park JH, Hong JH, Lee SW, Ji HD, Jung JA, Yoon KW, Lee JI, Won KS, Song BI, Kim HW. The effect of chronic cerebral hypoperfusion on the pathology of Alzheimer's disease: A positron emission tomography study in rats. Sci Rep. 2019; 9:14102.
https://doi.org/10.1038/s41598-019-50681-4
PMID:31575996

40. Aliev G, Obrenovich ME, Smith MA, Perry G. Hypoperfusion, Mitochondria Failure, Oxidative Stress, and Alzheimer Disease. J Biomed Biotechnol. 2003; 2003:162–63.
https://doi.org/10.1155/S1110724303305029
PMID:12975531

41. Poh L, Fann DY, Wong P, Lim HM, Foo SL, Kang SW, Rajeev V, Selvaraji S, Iyer VR, Parathy N, Khan MB, Hess DC, Jo DG, et al. AIM2 inflammasome mediates hallmark neuropathological alterations and cognitive impairment in a mouse model of vascular dementia. Mol Psychiatry. 2020. [Epub ahead of print].
https://doi.org/10.1038/s41380-020-00971-5
PMID:33299135

42. Manczak M, Jung Y, Park BS, Partovi D, Reddy PH. Time-course of mitochondrial gene expressions in mice brains: implications for mitochondrial dysfunction, oxidative damage, and cytochrome c in aging. J Neurochem. 2005; 92:494–504.
https://doi.org/10.1111/j.1471-4159.2004.02884.x
PMID:15659220

43. Danyu L, Yanran L, Xiuna J, Ying C, Sudan P, Tianen Z, Zhifen Z, Dezhi Z, Kaixun H, Yingyu X, Enxiang T. α-Synuclein induced mitochondrial dysfunction via cytochrome c oxidase subunit 2 in SH-SY5Y cells. Exp Cell Res. 2019; 378:57–65.
https://doi.org/10.1016/j.yexcr.2019.02.006
PMID:30776354

44. Sgobio C, Wu J, Zheng W, Chen X, Pan J, Salinas AG, Davis MI, Lovinger DM, Cai H. Aldehyde dehydrogenase 1-positive nigrostriatal dopaminergic fibers exhibit distinct projection pattern and dopamine release dynamics at mouse dorsal striatum. Sci Rep. 2017; 7:5283.
https://doi.org/10.1038/s41598-017-05598-1
PMID:28706191

45. Wey MC, Fernandez E, Martinez PA, Sullivan P, Goldstein DS, Strong R. Neurodegeneration and motor dysfunction in mice lacking cytosolic and mitochondrial aldehyde dehydrogenases: implications for Parkinson's disease. PLoS One. 2012; 7:e31522.
https://doi.org/10.1371/journal.pone.0031522
PMID:22384032

46. Arumugam TV, Phillips TM, Cheng A, Morrell CH, Mattson MP, Wan R. Age and energy intake interact to modify cell stress pathways and stroke outcome. Ann Neurol. 2010; 67:41–52.
https://doi.org/10.1002/ana.21798
PMID:20186857

47. Scior A, Buntru A, Arnsburg K, Ast A, Iburg M, Juenemann K, Pigazzini ML, Mlody B, Puchkov D, Priller J, Wanker EE, Prigione A, Kirstein J. Complete suppression of Htt fibrilization and disaggregation of Htt fibrils by a trimeric chaperone complex. EMBO J. 2018; 37:282–99.
https://doi.org/10.15252/embj.201797212
PMID:29212816

48. O'Brien R, DeGiacomo F, Holcomb J, Bonner A, Ring KL, Zhang N, Zafar K, Weiss A, Lager B, Schilling B, Gibson BW, Chen S, Kwak S, Ellerby LM. Integration-independent Transgenic Huntington Disease Fragment Mouse Models Reveal Distinct Phenotypes and Life Span *in Vivo*. J Biol Chem. 2015; 290:19287–306.
https://doi.org/10.1074/jbc.M114.623561
PMID:26025364

49. Zhang M, Qian C, Zheng ZG, Qian F, Wang Y, Thu PM, Zhang X, Zhou Y, Tu L, Liu Q, Li HJ, Yang H, Li P, Xu X. Jujuboside A promotes Aβ clearance and ameliorates cognitive deficiency in Alzheimer's disease through activating Axl/HSP90/PPARγ pathway. Theranostics. 2018; 8:4262–78.
https://doi.org/10.7150/thno.26164 PMID:30128052

50. Wolf G, Lotan A, Lifschytz T, Ben-Ari H, Kreisel Merzel T, Tatarskyy P, Valitzky M, Mernick B, Avidan E, Koroukhov N, Lerer B. Differentially Severe Cognitive Effects of Compromised Cerebral Blood Flow in Aged Mice: Association with Myelin Degradation and Microglia Activation. Front Aging Neurosci. 2017; 9:191.
https://doi.org/10.3389/fnagi.2017.00191
PMID:28670274

51. Pellizzoni L. Chaperoning ribonucleoprotein biogenesis in health and disease. EMBO Rep. 2007; 8:340–45. https://doi.org/10.1038/sj.embor.7400941 PMID:17401408

52. Liu MY, Nemes A, Zhou QG. The Emerging Roles for Telomerase in the Central Nervous System. Front Mol Neurosci. 2018; 11:160. https://doi.org/10.3389/fnmol.2018.00160 PMID:29867352

53. Turi Z, Lacey M, Mistrik M, Moudry P. Impaired ribosome biogenesis: mechanisms and relevance to cancer and aging. Aging (Albany NY). 2019; 11:2512–40. https://doi.org/10.18632/aging.101922 PMID:31026227

54. Narla A, Ebert BL. Ribosomopathies: human disorders of ribosome dysfunction. Blood. 2010; 115:3196–205. https://doi.org/10.1182/blood-2009-10-178129 PMID:20194897

55. Bundy JL, Vied C, Nowakowski RS. Sex differences in the molecular signature of the developing mouse hippocampus. BMC Genomics. 2017; 18:237. https://doi.org/10.1186/s12864-017-3608-7 PMID:28302071

56. Haghani A, Johnson RG, Woodward NC, Feinberg JI, Lewis K, Ladd-Acosta C, Safi N, Jaffe AE, Sioutas C, Allayee H, Campbell DB, Volk HE, Finch CE, Morgan TE. Adult mouse hippocampal transcriptome changes associated with long-term behavioral and metabolic effects of gestational air pollution toxicity. Transl Psychiatry. 2020; 10:218. https://doi.org/10.1038/s41398-020-00907-1 PMID:32636363

57. Podcasy JL, Epperson CN. Considering sex and gender in Alzheimer disease and other dementias. Dialogues Clin Neurosci. 2016; 18:437–46. https://doi.org/10.31887/DCNS.2016.18.4/cepperson PMID:28179815

SUPPLEMENTARY MATERIALS

Supplementary Figures

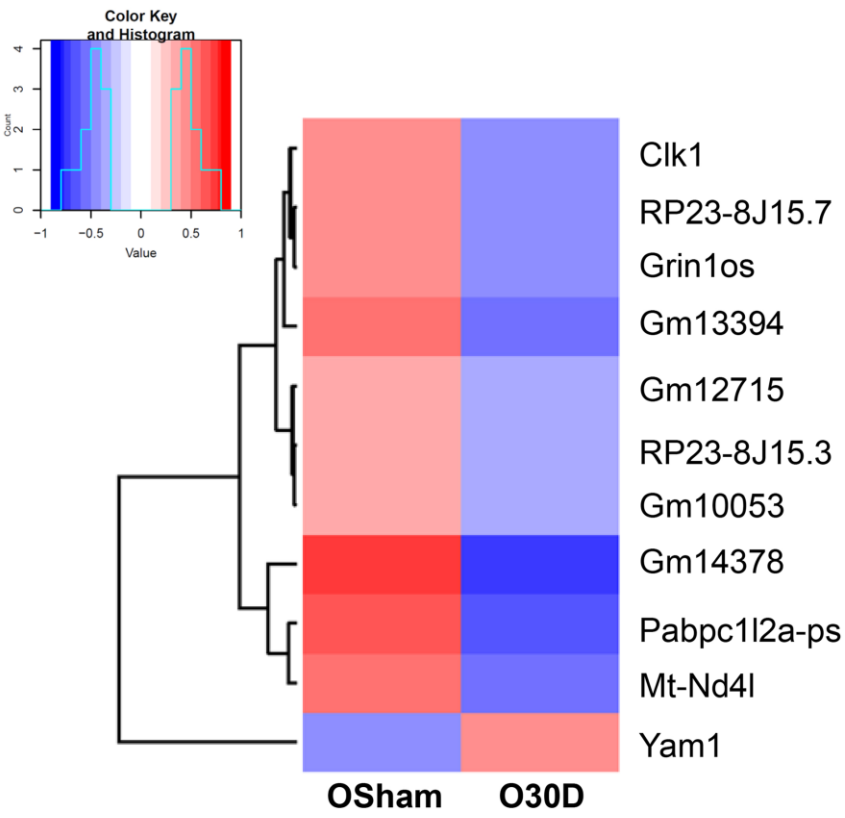

Supplementary Figure 1. Hierarchical clustering analysis of all 11 differentially expressed genes in O30D compared to OSham mice. There were no significant DEGs in O7D compared to OSham mice and hence is not represented in the heatmap. Upregulated gene expression is represented in red and downregulated gene expression in blue. The colour scale represents the log10 (average FPKM+1) value.

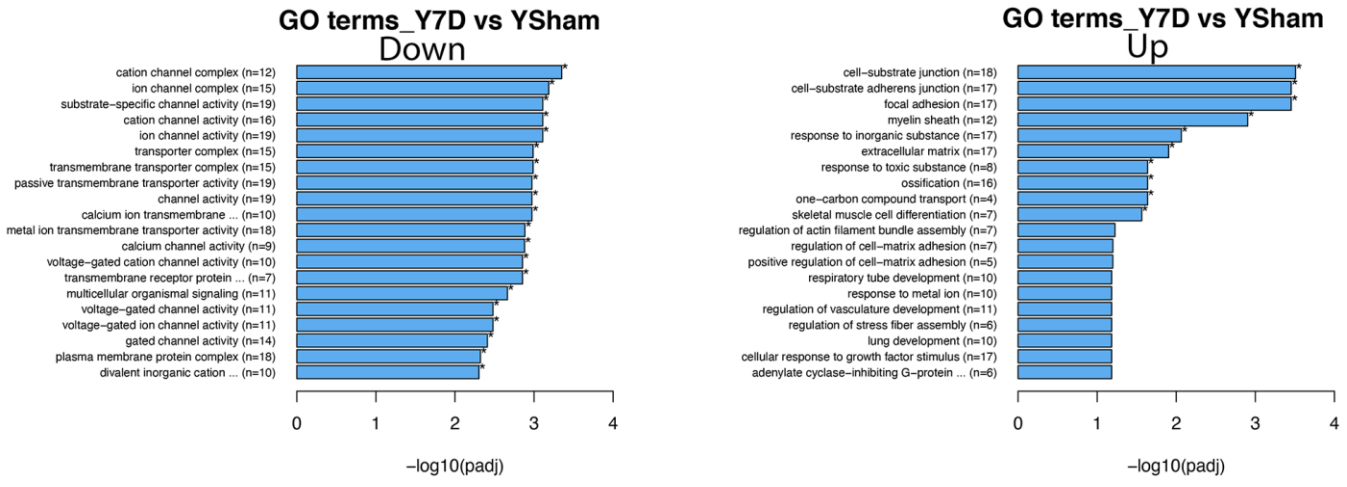

Supplementary Figure 2. Significant GO terms in Y7D vs YSham mice (q < 0.05). The horizontal axis represents the -log10 scale for q-value of each GO term.

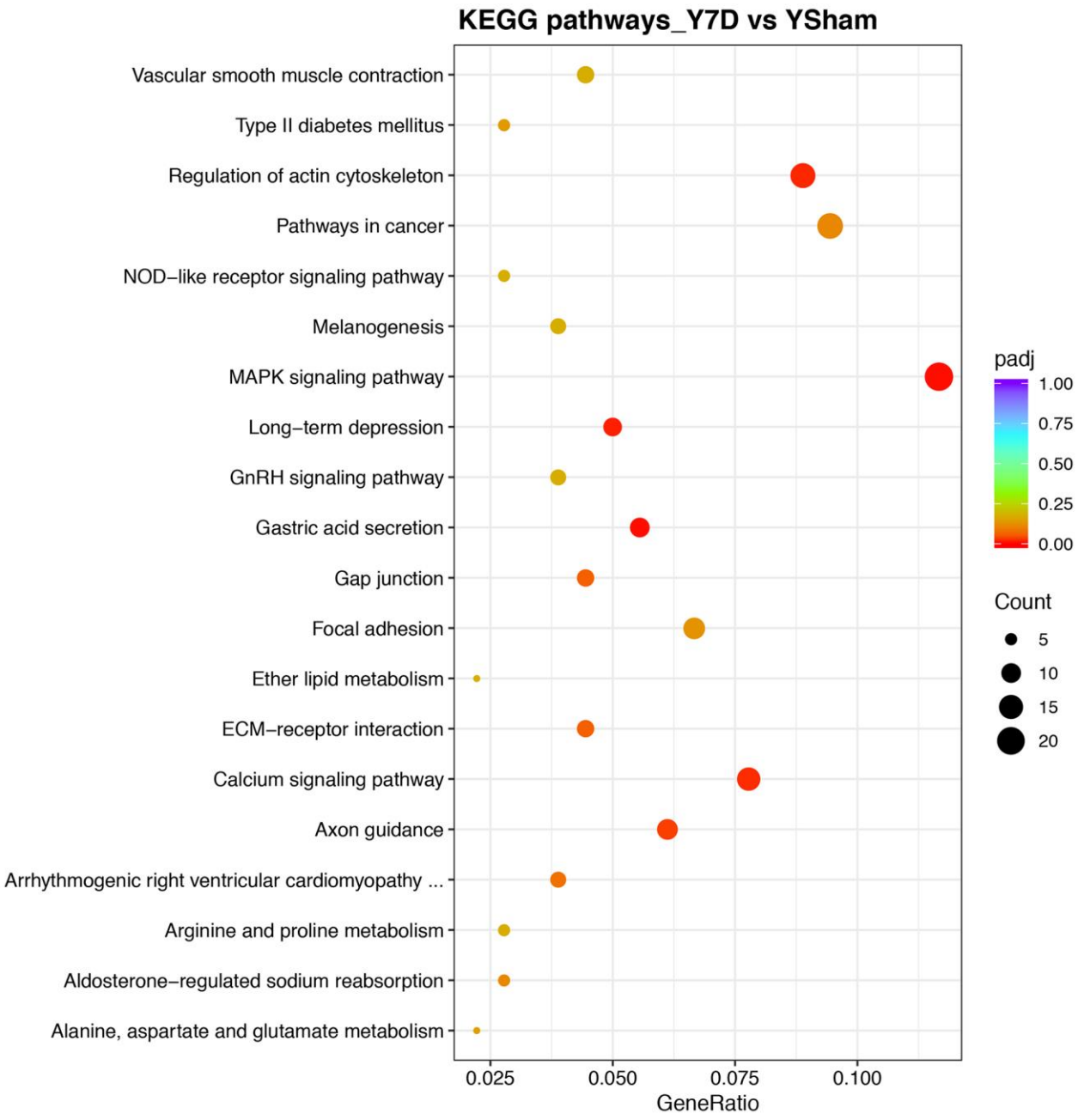

Supplementary Figure 3. KEGG pathway enrichment analysis between Y7D and YSham mice. The size of the dots represents the gene ratio involvement and the colour represents the significance. Red represents most significant and purple represents the least significant with the gradient showing the q-value range.

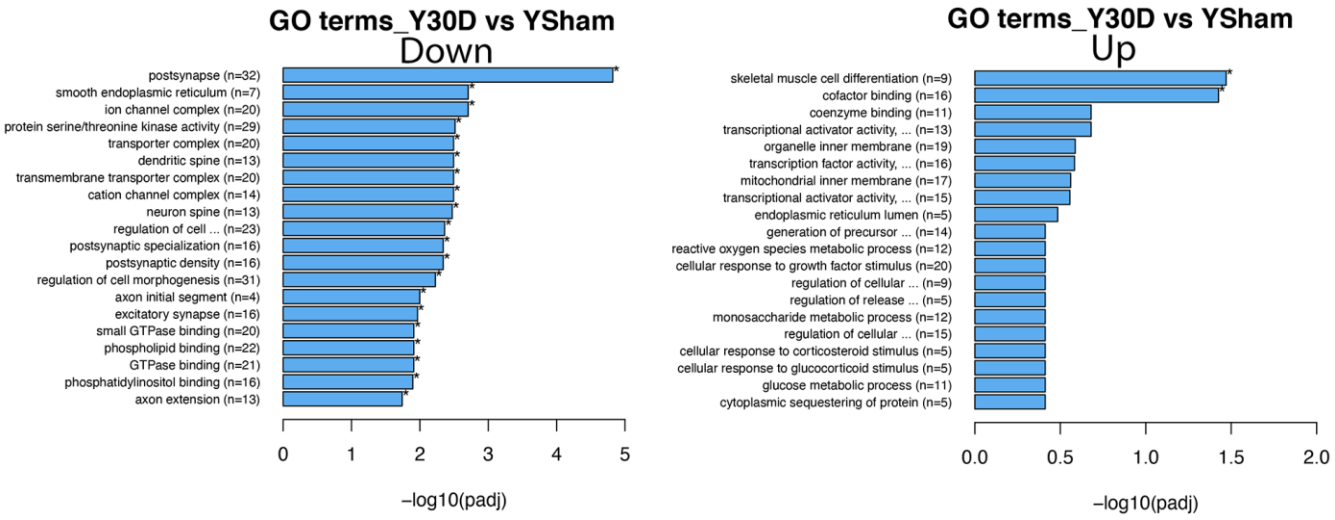

Supplementary Figure 4. Significant GO terms in Y30D vs YSham mice (q < 0.05). The horizontal axis represents the -log10 scale for q-value of each GO term.

Supplementary Tables

Please browse Full Text version to see the data of Supplementary Tables 1–3, 6.

Supplementary Table 1. List of all significantly (q<0.05) enriched upregulated and downregulated GO terms for old Sham against young Sham animals.

Supplementary Table 2. List of all differentially expressed (upregulated and downregulated) genes in old Sham against young Sham animals.

Supplementary Table 3. List of all differentially expressed (upregulated and downregulated) genes in mice subjected to 7 and 30 days of BCAS.

Supplementary Table 4. List of all KEGG pathways under the pathway enrichment analysis for mice subjected to 7 and 30 days of BCAS.

Description	ID	q-value	geneID	Count
MAPK signaling pathway	mmu04010	0.002396	Gna12/Cacna1e/Hspa1l/Gadd45b/Fos/Gadd45g/Rasgrf2/Cacna2d3/Nr4a1/Cacna1h/Dusp1/Pdgfrb/Fgfr2/Ikbkb/Pla2g3/Ntf3/Prkca/Prkcb/Fgfr3/Cacnb2/Mapk3	21
Gastric acid secretion	mmu04971	0.00249	Car2/Itpr2/Gnai2/Plcb2/Kcnj2/Chrm3/Sstr2/Prkca/Ezr/Prkcb	10
Long-term depression	mmu04730	0.007753	Gna12/Itpr2/Ryr1/Gnai2/Pla2g3/Plcb2/Prkca/Prkcb/Mapk3	9
Regulation of actin cytoskeleton	mmu04810	0.011272	Gna12/Itgb4/Iqgap2/Pdgfrb/Fn1/Gsn/Nckap1/Fgfr2/Itga11/Itga9/Chrm4/Chrm3/Ezr/Fgfr3/Mapk3/Chrm5	16
Calcium signaling pathway	mmu04020	0.013768	Cacna1e/Plcg1/Cacna1h/Pdgfrb/Phkg1/Itpr2/Ryr1/Phka1/Drd5/Plcb2/Chrm3/Prkca/Prkcb/Chrm5	14
Axon guidance	mmu04360	0.026275	Efnb3/Sema6a/Slit1/Epha7/Sema3c/Plxna4/Srgap3/Gnai2/Epha6/Mapk3/Sema3e	11

Supplementary Table 5. List of all significantly (q<0.05) enriched upregulated and downregulated GO terms for mice subjected to 7 and 30 days of BCAS.

Description	ID	Category	q-value
cellular response to growth factor stimulus	GO:0071363	BP	0.007679
positive regulation of endothelial cell migration	GO:0010595	BP	0.007679
regulation of endothelial cell migration	GO:0010594	BP	0.009149
endothelial cell migration	GO:0043542	BP	0.009149
positive regulation of neuron death	GO:1901216	BP	0.009149
posttranscriptional regulation of gene expression	GO:0010608	BP	0.009149
regulation of cell morphogenesis	GO:0022604	BP	0.009149
protein serine/threonine kinase activity	GO:0004674	MF	0.015801
negative regulation of protein phosphorylation	GO:0001933	BP	0.023866
modulation of synaptic transmission	GO:0050804	BP	0.023866
postsynapse	GO:0098794	CC	0.026809
negative regulation of protein modification process	GO:0031400	BP	0.029445
regulation of cellular amide metabolic process	GO:0034248	BP	0.029445
regulation of mitochondrial fission	GO:0090140	BP	0.033902
negative regulation of phosphorylation	GO:0042326	BP	0.048738

Supplementary Table 6. List of all common differentially expressed (upregulated and downregulated) genes in mice subjected to 7 and 30 days of BCAS.